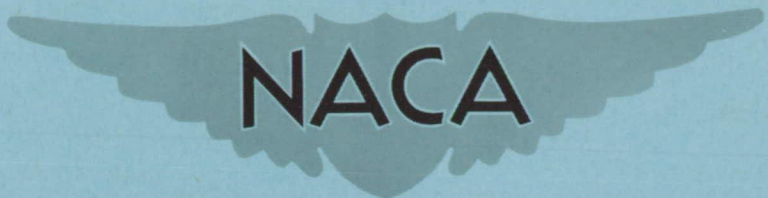


~~CONFIDENTIAL~~

Copy 91
RM L52D23a



NACA

RESEARCH MEMORANDUM

CLASSIFICATION CHANGED TO Unclassified
BY AUTHORITY OF NASA Bull. #74
ON 2/1/67 OF JR

A THEORETICAL AND EXPERIMENTAL INVESTIGATION OF THE LIFT
AND DRAG CHARACTERISTICS OF A HYDROFOIL AT
SUBCRITICAL AND SUPERCRITICAL SPEEDS

By Kenneth L. Wadlin, Charles L. Shuford, Jr.
and John R. McGehee

Langley Aeronautical Laboratory
Langley Field, Va.

ENGINEERING DEPT. LIBRARY
CHANCE-VOUGHT AIRCRAFT
DALLAS, TEXAS

~~CONFIDENTIAL~~

This material contains information affecting the National Defense of the United States within the meaning of the espionage laws, Title 18, U.S.C., sections 793 and 794, the transmission or revelation of which in any manner to an unauthorized person is prohibited by law.

NATIONAL ADVISORY COMMITTEE FOR AERONAUTICS

WASHINGTON
July 14, 1952

~~CONFIDENTIAL~~

JUL 18 1952

1-5

NATIONAL ADVISORY COMMITTEE FOR AERONAUTICS

RESEARCH MEMORANDUM

A THEORETICAL AND EXPERIMENTAL INVESTIGATION OF THE LIFT
AND DRAG CHARACTERISTICS OF A HYDROFOIL AT
SUBCRITICAL AND SUPERCRITICAL SPEEDS

By Kenneth L. Wadlin, Charles L. Shuford, Jr.
and John R. McGehee

SUMMARY

A theoretical and experimental investigation was made of the effect of the free-water surface and rigid boundaries on the lift and drag of an aspect-ratio-10 hydrofoil at both subcritical and supercritical speeds. The experimental investigation was made in Langley tank no. 1 and Langley tank no. 2 at 0.84 and 3.84 chords submergence at subcavitation speeds from 5 to 45 feet per second corresponding to Reynolds numbers from 0.18×10^6 to 1.64×10^6 .

Approximate theoretical solutions for the effects of the free-water surface and rigid boundaries on lift and drag at supercritical speeds are developed. An approximate theoretical solution for the effects of these boundaries on drag at subcritical speeds is also presented. The agreement between theory and experiment at both supercritical and subcritical speeds is satisfactory for engineering calculations of hydrofoil characteristics from aerodynamic data.

The experimental investigation indicated no appreciable effect of the limiting speed of wave propagation on lift-curve slope or angle of zero lift. It also showed that the increase in drag as the critical speed is approached from the supercritical range is gradual. This result is contrary to the abrupt increase at the critical speed predicted by theory.

INTRODUCTION

Airfoils and hydrofoils operate in fluids which differ principally in density and viscosity, properties that are readily treated by the concept of Reynolds number. Since such is true, the vast amount of

aerodynamic data already accumulated becomes available for use in predicting hydrofoil characteristics. However, the airfoil generally operates in an essentially infinite medium, whereas hydrofoil applications usually require operation in a limited medium, that is, in the proximity of the water surface. Aside from the effects of cavitation then, the principal difference between airfoil and hydrofoil applications is one of boundaries.

In restricted areas such as shallow harbors, canals, and towing tanks other boundaries are present besides the water surface, that is, the bottom and sides. Naturally these boundaries also influence the characteristics of a hydrofoil and their effects must be evaluated to use aerodynamic data for the prediction of the characteristics of hydrofoils under such conditions.

In addition to the reflective influence of the bottom and sides the finite depth of water limits the speed of propagation of the transverse waves generated by the hydrofoil. This change in flow causes the lift and drag characteristics to be different at speeds below this limiting or "critical speed" than they are above it.

In the present paper available aerodynamic and hydrodynamic theories have been applied to develop an approximate method of evaluating the influence of boundaries in order to apply existing aerodynamic data to hydrofoils and to correct properly data obtained in towing tanks to actual open-water conditions.

Experimental data were obtained in two water depths at two depths of submergence at both subcritical and supercritical speeds and compared with aerodynamic data corrected for the boundaries. The boundary-correction methods employed are similar to the general methods used in wind-tunnel research with the additional consideration that the limiting speed of wave propagation is taken into account.

SYMBOLS

L	lift of the hydrofoil, lb
L_1	lift at infinite submergence, lb
L_2	lift at finite submergence, lb
D	drag, lb
D_1	drag at infinite submergence, lb

D_2	drag at finite submergence, lb
D_3	wave drag, lb
C_L	lift coefficient, $\frac{L}{qS}$
C_{L1}	lift coefficient at infinite submergence, $\frac{L_1}{qS}$
C_{L2}	lift coefficient at finite submergence, $\frac{L_2}{qS}$
C_D	drag coefficient, $\frac{D}{qS}$
C_{D1}	drag coefficient at infinite submergence, $\frac{D_1}{qS}$
C_{D2}	drag coefficient at finite submergence, $\frac{D_2}{qS}$
C_{D3}	wave drag coefficient, $\frac{D_3}{qS}$
c_d	section drag coefficient
C_{Di}	induced drag coefficient of a rectangular hydrofoil in an infinite fluid
δC_{Di}	induced drag coefficient due to the trailing-vortex images
ΔC_{Di}	induced drag coefficient due to the horseshoe-vortex images
S	area of hydrofoil, sq ft
q	free-stream dynamic pressure, $\frac{1}{2} \rho V^2$, lb/sq ft
V	free-stream velocity, ft/sec
V_c	limiting speed of wave propagation or "critical speed," ft/sec
ρ	mass density, slugs/cu ft
ν	kinematic viscosity, ft ² /sec
g	acceleration due to gravity, ft/sec ²

c_{l_0}	section lift coefficient at infinite submergence
c_l	section lift coefficient at finite submergence
a_{01}	section lift-curve slope at infinite submergence, $\frac{dc_{l_0}}{d\alpha_0}$
a_{02}	section lift-curve slope at finite submergence, $\frac{dc_l}{d\alpha_0}$
a_1	slope of lift curve at infinite submergence, $\frac{dC_{L1}}{d\alpha}$
a_2	slope of lift curve at finite submergence, $\frac{dC_{L2}}{d\alpha}$
α	angle of attack, deg
α_0	section angle of attack, deg
Γ	circulation strength of vortex, $\frac{VcC_L}{2}$
Γ_1	circulation strength of vortex at infinite submergence
Γ_2	circulation strength of vortex at finite submergence
W_1	induced vertical velocity at three-quarter chord due to bound vortex of hydrofoil (surface boundary only)
W_2	induced vertical velocity at three-quarter chord due to hydrofoil image bound vortex (surface boundary only)
W_3	induced vertical velocity at three-quarter chord due to two trailing vortices of hydrofoil (surface boundary only)
W_4	induced vertical velocity at three-quarter chord due to two hydrofoil-image trailing vortices (surface boundary only)
W_5	induced vertical velocity at three-quarter chord due to horseshoe vortex of the hydrofoil

W_6	induced vertical velocity at three-quarter chord due to hydrofoil-image horseshoe vortex (surface boundary only)
W_7	induced vertical velocity at three-quarter chord due to hydrofoil-image bound vortices (multiple boundaries)
W_8	induced vertical velocity at three-quarter chord due to hydrofoil-image trailing vortices (multiple boundaries)
c	chord of hydrofoil, ft
h	depth of water, ft
f	depth of quarter chord of hydrofoil below free-water surface, ft
x	distance of the bound vortex measured in free-stream direction from three-quarter chord of the hydrofoil, ft
y	distance to center of image horseshoe vortex, measured parallel to the lifting line, from the center of the hydrofoil, ft
z	distance of image bound vortex, measured normal to the water surface, from the hydrofoil quarter-chord point, ft
b	semispan of hydrofoil, ft
A	geometric aspect ratio, $\frac{2b}{c}$
σ	plan-form correction factor for rectangular wings (see ref. 9)
E_e	effective edge-velocity correction for lift
R	Reynolds number, $\frac{Vc}{\nu}$
F	Froude number based on depth of hydrofoil submergence, $\frac{v^2}{gf}$

DESCRIPTION OF MODEL

The experimental data were obtained by using an 8-inch-chord hydrofoil with an aspect ratio of 10 supported by an 8-inch-chord strut intersecting the upper surface of the hydrofoil without fillets. The strut was perpendicular to the chord of the hydrofoil. The hydrofoil and struts were made of stainless steel. They were polished to a smooth finish consistent with current wind-tunnel practice.

The sections of the hydrofoil and strut were the same as those used in references 1 and 2. The hydrofoil had an NACA 64₁A412 section which differs from the NACA 64₁-412 section only by elimination of the trailing-edge cusp; the section characteristics of these two are essentially the same (see ref. 3). The strut had an NACA 66₁-012 section. Table 1 gives the ordinates for the hydrofoil and strut sections as computed from references 3 and 4.

APPARATUS AND PROCEDURE

The tests were made in both Langley tank no. 1 and tank no. 2 to obtain two water depths. Figure 1 shows a view of the test setup with the hydrofoil and balance attached to the structure on the Langley tank no. 2 carriage. The setup in Langley tank no. 1 was similar except for the method of attachment to the carriage. Figure 2 shows the cross sections of the two tanks. Tank no. 1 has a mean depth of 10.64 feet; tank no. 2 has a uniform depth of 6.0 feet.

The hydrofoil was moved vertically by means of a motor-driven jacking screw which moved the balance and hydrofoil as a unit. Change in angle of attack was obtained at the plate attaching the strut to the balance.

Measurements of lift and drag were made by means of electrical strain gages. The force measurements were made at constant speed, angle of attack, and depth of submergence. The depth of submergence is defined as the distance from the undisturbed water surface to the quarter-chord point on the chord line. This definition differs from that of references 1 and 2. The numerical difference is approximately 0.7 inch or 0.09 chord greater depth with the present definition than the previous one. The present definition is more suitable for use in the theory. Tests were made at two submergences (0.84 chord and 3.84 chords), over a range of speeds from 5 to 45 feet per second, and a range of angles of attack from -3.5° to 6.0° . The change in angle of

attack due to structural deflection caused by the lift and drag forces on the hydrofoil was obtained during the calibration of the balance and the test data were adjusted accordingly.

The supporting strut was run alone at the same range of speeds, depths, and angles as the combination. For these tests the end of the strut was fitted with a faired cap. The tares thus obtained were deducted from the test data to give the net forces. The net forces were converted to the usual aerodynamic lift and drag coefficients by using a measured value of ρ of 1.966 slugs per cubic foot at the testing temperatures which were 40° F for the tests at 0.84-chord submergence in Langley tank no. 1 and 44° F for all other tests in both tanks. All coefficients were based on the area of the hydrofoil. The area of the hydrofoil used in the present tests is 4.44 square feet. The measured kinematic viscosity of the water at the time of the tests in tank no. 1 at 40° F was 1.85×10^{-5} feet squared per second, in tank no. 1 at 44° F was 1.73×10^{-5} feet squared per second, and in tank no. 2 at 44° F was 1.83×10^{-5} feet squared per second.

EXPERIMENTAL RESULTS

The basic experimental results corrected for strut deflection and drag tares are presented in figure 3 as curves of lift and drag for each water depth and depth of hydrofoil submergence plotted against angle of attack with speed as the parameter. The data, converted to coefficients, are presented in figure 4 in the usual form for aerodynamic data. The strut-drag coefficients (based on the area of the hydrofoil, 4.44 ft²) plotted against speed are shown in figure 5.

The lift-curve slopes and angles of zero lift from figure 4 are plotted against Reynolds number in figure 6. Also included in this figure are the corresponding aerodynamic data for the NACA 653-418 section. These data were taken from reference 5 and the lift-curve slopes were corrected to aspect ratio 10 by the equation

$$a_1 = \frac{Aa_{o1}}{AE_e + \frac{57.3}{\pi} a_{o1}} \quad (1)$$

from reference 6 where E_e is an effective-edge-velocity correction from reference 7. The hydrofoil data show no significant effect of tank depth at either depth of submergence. It is of particular interest to note that, where this effect would be expected to be most pronounced, that is, in the region between the dashed vertical lines of figure 6 where the speed in tank no. 1 is subcritical while that in tank no. 2

is supercritical, the lift-curve slope and angle of zero lift for a given Reynolds number are essentially the same for both tanks. In the region below the critical speeds the trends are not too apparent. The lift-curve slopes decrease and the angles of zero lift increase with decreasing Reynolds number, particularly at the shallower depth of submergence. Such a tendency is indicated by the corresponding low Reynolds number aerodynamic data for the NACA 65₃-418 section. The reason for the variation of this tendency with depth of submergence is not fully understood; however, changes in pressure distribution due to changes in submergence would influence the Reynolds number effect. It appears therefore that if the lift-curve slopes and angles of zero lift are influenced by the critical speed the influence indicated by these tests is so small as to be masked by Reynolds number effects encountered in the tests and by the effects of submergence.

The variation of drag coefficient with speed for the 10.64 feet and the 6.0 feet water depths at lift coefficients of 0.4 and 0.6 and depths of submergence of 0.84 and 3.84 chords and aerodynamic section drag data at the same lift coefficients for the NACA 65₃-418 airfoil section from reference 5 are shown in figure 7. A comparison of the drag coefficients for the two water depths at both lift coefficients and both depths of submergence shows that, with reducing speed, when the critical speed in the greater water depth (tank no. 1, 15.98 chords) was approached, a drag rise occurred whereas the drag in the shallower water depth (tank no. 2, 9 chords) did not rise until its lower critical speed was approached. It can be seen that the drag rise increases with lift coefficient and decreases with depth of submergence as is predicted by the theory that will be discussed later. The trends at the low subcritical speeds are not too clear since they are masked by Reynolds number effects. An indication of the possible Reynolds number effects can be obtained from the aerodynamic data presented.

THEORETICAL BOUNDARY CORRECTIONS - SUPERCRITICAL

General

In order to use aerodynamic data for an airfoil in an infinite medium to predict the characteristics of a hydrofoil in the proximity of the water surface and perhaps also rigid boundaries as would be encountered in shallow water, canals, or towing tanks, the influence of these boundaries must be evaluated. The boundary condition to be satisfied at the free surface is that of constant pressure along the surface streamlines. The boundary condition to be satisfied at the rigid boundaries is zero normal velocity.

Free-Surface Boundary

As a first approximation to the three-dimensional problem supercritical conditions are assumed, however with only the free-water-surface boundary present. The constant-pressure boundary at the free surface can be satisfied by the introduction of a horseshoe vortex above the surface which has the same direction of rotation as the one which represents the loading on the hydrofoil (fig. 8).

The presence of the image bound vortex does not change the direction of the flow relative to the hydrofoil chord line in the vicinity of the center of pressure, but it does tend to curve the streamlines relative to the hydrofoil chord line. The curvature effect is equivalent to introducing camber of the hydrofoil in such a manner as to produce a negative lift increment. It would seem therefore that a reasonably close approximation to the effect of the free surface could be obtained by simply evaluating the effect of streamline curvature, in addition to the induced-angle effect of the trailing vortices, by applying a technique frequently used in approximate solutions of aerodynamic problems (see ref. 8). This technique involves determination of the circulation Γ required to produce a downward velocity $W_5 + W_6$ at the three-quarter-chord location which when combined with the free-stream velocity V produces a flow tangent to the mean camber line of the hydrofoil. Thus, if geometric camber is neglected, the hydrofoil angle of attack α is equal to the sum of the angles at the three-quarter-chord point induced by the hydrofoil vortices and their images located at a distance directly above the hydrofoil equal to twice the depth of submergence.

By use of the Biot-Savart law and the notations defined in figure 8 the following expressions for the separate contributions at the line of symmetry to the vertical component of the induced velocity at the three-quarter chord were obtained:

$$W_1 = \frac{\Gamma}{\pi c} \left[\frac{b}{\sqrt{\left(\frac{c}{2}\right)^2 + b^2}} \right] \quad (2)$$

due to the bound vortex of the hydrofoil,

$$W_2 = \frac{\Gamma}{4\pi \left[\left(\frac{c}{2}\right)^2 + (2f)^2 \right]} \left[\frac{bc}{\sqrt{\left(\frac{c}{2}\right)^2 + (2f)^2 + b^2}} \right] \quad (3)$$

due to the image bound vortex,

$$W_3 = \frac{\Gamma}{2\pi b} \left[\frac{c}{2\sqrt{\left(\frac{c}{2}\right)^2 + b^2}} + 1 \right] \quad (4)$$

due to the two trailing vortices of the hydrofoil,

$$W_4 = \frac{\Gamma b}{2\pi [b^2 + (2f)^2]} \left[\frac{c}{2\sqrt{\left(\frac{c}{2}\right)^2 + b^2 + (2f)^2}} + 1 \right] \quad (5)$$

due to the two image trailing vortices,

$$W_5 = \frac{\Gamma}{2\pi} \left[\frac{2}{bc} \sqrt{\left(\frac{c}{2}\right)^2 + b^2} + \frac{1}{b} \right] \quad (6)$$

due to the horseshoe vortex of the hydrofoil and

$$W_6 = \frac{\Gamma}{4\pi} \left\{ \left[\frac{c}{\left(\frac{c}{2}\right)^2 + (2f)^2} \right] \left[\frac{b}{\sqrt{\left(\frac{c}{2}\right)^2 + (2f)^2 + b^2}} \right] + \frac{2b}{(2f)^2 + b^2} \left[1 + \frac{c}{2\sqrt{\left(\frac{c}{2}\right)^2 + (2f)^2 + b^2}} \right] \right\} \quad (7)$$

due to the image horseshoe vortex.

By means of equations (6) and (7) a computation of the angle of attack α can be made.

Effect on lift.- In order to estimate the effect of depth of submergence on lift the ratio of the hydrofoil circulation in an infinite fluid to that of a hydrofoil at a finite depth of submergence for a given angle of attack is obtained. That is:

$$\frac{\Gamma_1}{\Gamma_2} = \frac{W_5 + W_6}{W_5} = 1 + \frac{W_6}{W_5} \quad (8)$$

Therefore (for small angles),

$$\frac{\Gamma_1}{\Gamma_2} = 1 + \left\{ \frac{\frac{bc}{2\sqrt{\left(\frac{c}{2}\right)^2 + (2f)^2 + b^2}} \left[\frac{1}{\left(\frac{c}{2}\right)^2 + (2f)^2} + \frac{1}{(2f)^2 + b^2} \right] + \frac{b}{(2f)^2 + b^2}}{\frac{2}{bc}\sqrt{b^2 + \left(\frac{c}{2}\right)^2} + \frac{1}{b}} \right\}$$

where

$$\Gamma = \frac{VcC_L}{2}$$

and

$$\frac{\Gamma_2}{\Gamma_1} = \frac{C_{L2}}{C_{L1}} = \frac{a_2}{a_1}$$

when this equation is divided through by c to get f in terms of c and with

$$A = \frac{2b}{c}$$

$$\frac{a_2}{a_1} = \frac{1}{1 + \left\{ \frac{\frac{A}{4\sqrt{\frac{1}{4} + 4\left(\frac{f}{c}\right)^2 + \frac{A^2}{4}}} \left[\frac{1}{\frac{1}{4} + 4\left(\frac{f}{c}\right)^2} + \frac{1}{\frac{A^2}{4} + 4\left(\frac{f}{c}\right)^2} \right] + \frac{1}{\frac{8}{A}\left(\frac{f}{c}\right)^2 + \frac{A}{2}}}{\frac{2}{A}\left(\sqrt{A^2 + 1} + 1\right)} \right\}} \quad (9)$$

which is the ratio of lift-curve slope at finite depth to that at infinite depth when only the free surface is considered.

For the two-dimensional case (see ref. 1) the ratio of the lift-curve slope at finite depth to that at infinite depth for a given angle of attack is

$$\frac{a_{o2}}{a_{o1}} = \frac{\left(\frac{f}{c}\right)^2 + 1}{\left(\frac{f}{c}\right)^2 + 2}$$

Effect on drag.- In order to estimate the effect of depth of submergence on the drag of a finite-span rectangular hydrofoil the drag induced by the hydrofoil images at a given angle of attack is obtained

$$\Delta C_{Di} = C_{L2} \frac{W_6}{V} (1 + \sigma) \quad (10)$$

This relation is not rigorous since it gives an induced drag in two-dimensional flow due to the influence of the bound vortex at the three-quarter chord. However, for the aspect ratios under consideration when the drag correction is determined in the usual manner, that is by evaluating the downwash at the quarter-chord, the drag predicted is too low. This condition is true even when the spanwise distribution of downwash is considered.

From equation (7)

$$\frac{W_6}{V} = \frac{\Gamma}{4\pi V} K$$

where

$$K = \frac{c}{\left(\frac{c}{2}\right)^2 + 4f^2} \left[\frac{b}{\sqrt{\left(\frac{c}{2}\right)^2 + 4f^2 + b^2}} \right] + \frac{2b}{4f^2 + b^2} \left[1 + \frac{c}{2\sqrt{\left(\frac{c}{2}\right)^2 + 4f^2 + b^2}} \right]$$

The drag coefficient of a rectangular hydrofoil in an infinite fluid is

$$C_{D1} = c_d + \frac{C_{L1}^2}{\pi A} (1 + \sigma)$$

The total drag coefficient of a rectangular hydrofoil at a given depth of submergence and angle of attack, therefore, is

$$C_D = c_d + C_{L2}^2 \left(\frac{1}{A\pi} + \frac{Kc}{8\pi} \right) (1 + \sigma) \quad (11)$$

Restricted Area

In order to estimate the effect of depth of submergence on the lift and drag of a hydrofoil in a restricted area such as a shallow harbor, a canal, or towing tank, a system of images (fig. 9) that satisfied the boundary conditions of constant pressure at the free-water surface and zero normal velocity at the rigid boundaries is required. The boundary-induced vertical velocities at the three-quarter chord are obtained by computing the combined effect of sufficient images to give the desired accuracy. An infinite array of images is, of course, required to give an exact value. Sufficient accuracy, however, can be obtained with a finite array of images. For example, if another row of images were added to the top and bottom and another column of images to each side of the horseshoe vortex arrangement shown in figure 9 (A = 10, tank no. 2, submergence = 0.84 chord) the additional images would cause a change of less than 1 percent in the total induced vertical velocity at the three-quarter chord of the hydrofoil. The general equation for this velocity for each image vortex (see ref. 9) is:

$$W_7 = \frac{\Gamma}{4\pi} \left\{ \frac{x}{x^2 + z^2} \left[\frac{y + b}{\sqrt{x^2 + z^2 + (y + b)^2}} - \frac{y - b}{\sqrt{x^2 + z^2 + (y - b)^2}} \right] \right\} \quad (12)$$

due to the image bound vortex and

$$W_8 = \frac{\Gamma}{4\pi} \left\{ \frac{y+b}{z^2 + (y+b)^2} \left[1 + \frac{x}{\sqrt{x^2 + z^2 + (y+b)^2}} \right] - \frac{y-b}{z^2 + (y-b)^2} \left[1 + \frac{x}{\sqrt{x^2 + z^2 + (y-b)^2}} \right] \right\} \quad (13)$$

due to two image trailing vortices where x , y , and z define the location of the image with respect to the intersection of the quarter-chord line and the line of symmetry of the hydrofoil (see fig. 8).

The ratio $\frac{a_2}{a_1}$ and the drag coefficient C_D are obtained as previously discussed by substituting $(W_7 + W_8)$ for W_6 in equations (8) and (10).

Some results calculated by applying the foregoing theoretical method to these tanks for estimating the effect of submergence on lift-curve slope are shown in figure 10 for three aspect ratios.

Comparison of Theory and Experiment

Lift.- The theoretical results presented in figure 10 are compared in figure 11 with the present experimental results for a hydrofoil of aspect ratio 10 and with experimental results given in references 1, 2, and 10 for hydrofoils of aspect ratio 10, 4, and 6, respectively. The ratio $\frac{a_2}{a_1}$ for the experimental lift-curve slopes for hydrofoils of aspect ratios 6 and 10 is the ratio of the lift-curve slope obtained at a given depth of submergence to the lift-curve slope (corrected for aspect ratio by equation (1)) as obtained from airfoil data (see refs. 11 and 12). The ratio $\frac{a_2}{a_1}$ for the experimental lift-curve slopes for the aspect-ratio-4 hydrofoil is the ratio of the lift-curve slope obtained at a given depth of submergence to the lift-curve slope at the greatest depth of submergence. This ratio was chosen in the case of the aspect-ratio-4 hydrofoil because the experimental lift-curve slope at the greatest depth of submergence was higher than the lift-curve slope (corrected for aspect ratio by equation (1)) given by airfoil data. If

the method used for the hydrofoils of aspect ratios 6 and 10 had been used the ratios would be greater than 1.0. The difference in lift-curve slope causing this is about five percent.

The agreement of the experimental results with results given by the theoretical method is generally good.

Drag.- Results calculated by the restricted-area theoretical method for estimating the effect of depth of submergence, on the drag coefficient are shown in figure 12 for hydrofoils of aspect ratio 10, 6, and 4. The magnitude of the increments indicates that a correction to airfoil drag coefficients must be made to predict hydrofoil characteristics at supercritical speeds.

Results calculated by the restricted-area method for both tank no. 1 and tank no. 2 are compared in figure 13 with the present experimental results for a hydrofoil of aspect ratio 10 and in figures 14, 15, and 16 with the experimental results given in references 1, 10, and 2 for hydrofoils of aspect ratios 10, 6, and 4, respectively. The agreement of the experimental results with results given by the theoretical method is in most cases good.

THEORETICAL BOUNDARY CORRECTIONS - SUBCRITICAL

General

The speed of propagation of transverse waves generated by the bound vortex of the hydrofoil is limited to a speed which is a function of water depth. This speed is defined by \sqrt{gh} where g is the gravitational constant and h is the water depth. When the hydrofoil operates below this limiting or "critical speed" the transverse waves travel along with the hydrofoil whereas above this speed the transverse waves no longer accompany the hydrofoil. It follows, therefore, that the induced effects on lift and drag due to these waves are present below critical speeds but not above. The diverging waves due to the trailing vortices are not subject to this limitation and their effect is present at both subcritical and supercritical speeds. The effect then, of the trailing vortices, may be computed to a first approximation in the same manner at subcritical and supercritical speeds. The effect of the bound vortex at subcritical speeds, however, is not the same as at supercritical speeds.

Figure 6 indicates that the expected effect of the critical speed on lift was either not present or so small as to be masked by the Reynolds number effects encountered in the tests and by the effects of

submergence. It may therefore be assumed that to a first approximation the influence of the boundaries on lift will be the same as for the super-critical case and that only the influence on drag need be considered.

Since the condition generally encountered in actual applications is that of great water depth most of the theoretical work has considered only this case. Mathematical investigations of the wave drag of a submerged body were made by Lamb, who studied the motion of a circular cylinder and a spherical body. More exact solutions of these problems were given by Havelock, who solved further problems, for instance, that of the motion of a submerged ellipsoid. L. N. Sretensky (ref. 13) approached the problem of the submerged cylinder for both infinite and finite water depths by assuming the existence of circulation. Kotchin (ref. 14) gave general formulas for the hydrodynamic forces acting on profiles of arbitrary shape in water of infinite depth. Keldish and Lavrentiev (ref. 15) considered the case of a two-dimensional "thin" airfoil in water of infinite depth. Vladimirov (ref. 16) considered the case of a three-dimensional hydrofoil in water of infinite depth. Recent work by Meyer (reference 17) considered a two-dimensional hydrofoil in both infinite and finite water depths and in reference 18 the case of a three-dimensional hydrofoil in water of infinite depth.

Drag

In order to estimate the effect of depth of submergence on drag the induced drag due to the hydrofoil trailing-vortex images and wave drag must be added to the drag in an infinite fluid.

The boundary-induced drag coefficient due to the image trailing vortices is

$$\delta C_{D_i} = C_L \frac{W_4}{V} (1 + \sigma) \quad (14)$$

From equation (5)

$$\frac{W_4}{V} = \frac{\Gamma}{4\pi V} K_1$$

where

$$K_1 = \frac{2b}{b^2 + (2f)^2} \left[\frac{c}{2\sqrt{b^2 + (2f)^2 + \left(\frac{c}{2}\right)^2}} + 1 \right]$$

for a free surface, and from equation (13)

$$K_1 = \frac{y + b}{z^2 + (y + b)^2} \left[1 + \frac{x}{\sqrt{x^2 + z^2 + (y + b)^2}} \right] - \frac{y - b}{z^2 + (y - b)^2} \left[1 + \frac{x}{\sqrt{x^2 + z^2 + (y - b)^2}} \right] \quad (15)$$

for a restricted area (tank no. 1 and tank no. 2).

The wave drag coefficient for a hydrofoil at a given depth of submergence and speed is (refs. 14, 17, and 18)

$$C_{D3} = \frac{C_{L2}^2}{2 \frac{v^2}{gc}} \psi \quad (16)$$

where

$$\psi = e^{-\frac{2}{F}} \quad (17)$$

for a two-dimensional hydrofoil in water of infinite depth (refs. 14 and 17) and

$$\psi = \frac{\sinh^2 \left[\left(1 - \frac{f}{h} \right) U_0 \right]}{\cosh^2 U_0 - \frac{gh}{v^2}} \quad (18)$$

(the parameter U_0 is obtained from the relations $\frac{v^2}{gh} = \frac{\tanh U_0}{U_0}$)

for a two-dimensional hydrofoil in water of finite depth (ref. 17) and

$$\psi = \frac{v^2}{gb} \int_{\Lambda_2 = -\frac{b}{f}}^{\frac{b}{f}} d\Lambda_2 \int_{\Lambda_1 = -\frac{2b}{f}}^{\frac{2b}{f}} \psi_2 \left(F, \arctan \frac{\Lambda_1}{2} \right) d\Lambda_1 \quad (19)$$

and

$$\psi_2(F, \theta) = \frac{1}{32} \left\{ \frac{e^{-\frac{1}{F}}}{F^2} \left[(1 + \cos^2 \theta) i H_0^{(1)} \left(\frac{i}{F \cos \theta} \right) \right] - \right. \\ \left. (2 \cos \theta + F \cos \theta \cos 2\theta) H_1^{(1)} \left(\frac{i}{F \cos \theta} \right) - \frac{\cos^2 \theta \cos 2\theta}{\pi} \right\}$$

where $H_0^{(1)}$ and $H_1^{(1)}$ are Hankel functions and

$$\theta = \arctan \left(\frac{b}{2f} \right)$$

for a three-dimensional hydrofoil in water of infinite depth (ref. 18).

The drag coefficient of a rectangular hydrofoil in an infinite fluid is

$$C_{D1} = c_d + \frac{C_{L2}^2}{\pi A} (1 + \sigma) \quad (20)$$

Therefore, the drag coefficient of a rectangular hydrofoil at a given depth of submergence, angle of attack, and speed is

$$C_D = c_d + C_{L2}^2 \left[\frac{1 + \sigma}{\pi A} + \frac{K_{1c}(1 + \sigma)}{8\pi} + \frac{1}{2} \frac{v^2}{gc} \psi \right] \quad (21)$$

Comparison of Theory and Experiment

Figures 17 and 18 compare the present experimental results for a hydrofoil of aspect ratio 10 with the results calculated from equation (21). The theoretical results were obtained by estimating the section drag c_d , and adding the calculated induced drag coefficient of a rectangular hydrofoil in an infinite fluid C_{D_i} , the boundary induced drag δC_{D_i} , and the wave drag coefficient C_{D_3} .

The drag coefficient c_d at low Reynolds number was estimated by extending the section drag data of the NACA 64₁-412 airfoil by comparison (fig. 19) with low Reynolds number data for the NACA 65₃-418 airfoil section. The boundary-induced drag coefficient δC_{D_i} (equation (14)) was obtained by calculating K_1 for tank no. 1 and K_1 for tank no. 2 from equation (15). The wave drag coefficient was computed from equation (16), where the values for ψ were calculated from equation (17) (infinite water depth, two-dimensional hydrofoil), equation (18) (finite water depth, two-dimensional hydrofoil), and equation (19) (infinite water depth, three-dimensional hydrofoil). The values for ψ obtained from equations (17), (18), and (19) are compared in figure 20.

Figures 17 and 18 indicate that the wave drag coefficient for water of infinite depth (two-dimensional hydrofoil) added to $C_{D_1} + \delta C_{D_i}$ (where $C_{D_1} = c_d + C_{D_i}$) gives a better approximation of the experimental drag coefficient of a hydrofoil at a given depth of submergence and speed than when wave drag is calculated for water of finite depth (two-dimensional hydrofoil) or for water of infinite depth (three-dimensional hydrofoil).

This result may be due to the fact that the wave-drag theories do not consider both the effect of water depth and the three-dimensional case simultaneously whereas the experimental values were at a finite water depth for an aspect-ratio-10 hydrofoil. Suitable experimental data for other aspect ratios and water depths are not presently available to aid in clarifying the discrepancy. The difference in the theoretical and experimental results at 5 feet per second could be an additional section drag increment since the section drag coefficient was estimated by an arbitrary method.

CONCLUSIONS

The results of the tank tests of the aspect-ratio-10 hydrofoil and the results calculated by theory and compared to experiment may be summarized as follows:

1. A method has been developed which makes it possible to calculate at subcavitation speeds, to engineering accuracy, the lift and drag characteristics of a hydrofoil from aerodynamic data. The method accounts for the effects of submergence of the hydrofoil below the free-water surface, the proximity of fixed boundaries, and the limiting speed of wave propagation due to limited water depth.
2. There was no appreciable effect of the limiting speed of wave propagation on lift-curve slope or angle of zero lift at the two depths of submergence investigated.
3. The increase in drag as the critical speed is approached from the supercritical range is gradual. This result is contrary to the abrupt increase at the critical speed predicted by theory.

Langley Aeronautical Laboratory
National Advisory Committee for Aeronautics
Langley Field, Va.

REFERENCES

1. Wadlin, Kenneth L., Fontana, Rudolph E., and Shuford, Charles L., Jr.: The Effect of End Plates, End Struts, and Depth of Submergence on the Characteristics of a Hydrofoil. NACA RM L51B13, 1951.
2. Wadlin, Kenneth L., Ramsen, John A., and McGehee, John R.: Tank Tests at Subcavitation Speeds of an Aspect-Ratio-10 Hydrofoil With a Single Strut. NACA RM L9K14a, 1950.
3. Loftin, Laurence K., Jr.: Theoretical and Experimental Data for a Number of NACA 6A-Series Airfoil Sections. NACA Rep. 903, 1948. (Supersedes NACA TN 1368.)
4. Abbott, Ira H., Von Doenhoff, Albert E., and Stivers, Louis S., Jr.: Summary of Airfoil Data. NACA Rep. 824, 1945. (Supersedes NACA ACR L5C05.)
5. Quinn, John H., Jr., and Tucker, Warren A.: Scale and Turbulence Effects on the Lift and Drag Characteristics of the NACA 65₃-418, $a = 1.0$ Airfoil Section. NACA ACR L4H11, 1944.
6. Swanson, Robert S., and Crandall, Stewart M.: Lifting-Surface-Theory Aspect-Ratio Corrections to the Lift and Hinge-Moment Parameters for Full-Span Elevators on Horizontal Tail Surfaces. NACA Rep. 911, 1948. (Supersedes NACA TN 1175.)
7. Swanson, Robert S., and Priddy, E. LaVerne: Lifting-Surface Theory Values of the Damping in Roll and of the Parameter Used in Estimating Aileron Stick Forces. NACA ARR L5F23, 1945.
8. Wieghardt, Karl: Chordwise Load Distribution of a Simple Rectangular Wing. NACA TM 963, 1940.
9. Glauert, H.: The Elements of Aerofoil and Airscrew Theory. Second ed., Cambridge Univ. Press, 1948, p. 159.
10. Benson, James M., and Land, Norman S.: An Investigation of Hydrofoils in the NACA Tank, I - Effect of Dihedral and Depth of Submersion. NACA ACR, Sept. 1942.
11. Stack, John: Tests of Airfoils Designed to Delay the Compressibility Burble. NACA Rep. 763, 1943. (Supersedes NACA TN 976.)

12. Loftin, Laurence K., Jr., and Smith, Hamilton A.: Aerodynamic Characteristics of 15 NACA Airfoil Sections at Seven Reynolds Numbers From 0.7×10^6 to 9.0×10^6 . NACA TN 1945, 1949.
13. Sretensky, L. N.: Motion of a Cylinder Under the Surface of a Heavy Fluid. NACA TM 1335, 1952.
14. Kotchin, N.: On the Wave-Making Resistance and Lift of Bodies Submerged in Water. NACA TM 1340, 1952.
15. Keldish, M., and Lavrentiev, M.: The Motion of an Aerofoil Below the Surface of a Heavy Fluid. Rep. No. 3452 (S. 365), British A.R.C., Mar. 17, 1938. (Translation of the Transactions of the Conference on the Theory of Wave Resistance, U.S.S.R. (Moscow) 1937.)
16. Vladimirov, A.: Approximate Hydrodynamic Design of a Finite Span Hydrofoil. NACA TM 1341, 1952.
17. Meyer, Rudolf X.: Two-Dimensional Vortex-Line Theory of a Hydrofoil Operating in Water of Finite Depth. Tech. Rep. HR-1, The Hydrofoil Corp., Nov. 29, 1950.
18. Meyer, R. X.: Three-Dimensional Vortex-Line Theory of a Hydrofoil Operating in Water of Large Depth. Part I: The Wave Drag of a Single Hydrofoil With Prescribed Lift-Distribution. Tech. Rep. HR-4, The Hydrofoil Corp., Feb. 7, 1951.

Table 1.- Ordinates at strut and hydrofoil in inches



Hydrofoil, NACA 64₁A112

Upper surface		Lower surface	
Station	Ordinate	Station	Ordinate
0.026	0.084	0.054	-0.067
.044	.104	.076	-.079
.082	.135	.118	-.096
.178	.194	.221	-.126
.376	.279	.424	-.164
.575	.346	.625	-.190
.790	.401	.810	-.211
1.176	.490	1.224	-.241
1.578	.559	1.622	-.261
1.981	.611	2.019	-.274
2.384	.648	2.416	-.281
2.788	.673	2.812	-.281
3.192	.684	3.208	-.275
3.595	.679	3.605	-.259
3.999	.661	4.001	-.236
4.398	.632	4.402	-.207
4.795	.592	4.805	-.176
5.192	.544	5.208	-.142
5.590	.487	5.610	-.108
5.988	.422	6.012	-.076
6.386	.349	6.414	-.050
6.786	.265	6.814	-.034
7.190	.179	7.210	-.022
7.595	.090	7.605	-.012
8.000	.002	8.000	-.002
L.E. radius: 0.083		Slope of radius through L.E.: 0.168	



Strut, NACA 66₁-012

Station	Ordinate
0	0
.040	.072
.060	.087
.100	.109
.200	.145
.400	.200
.600	.243
.800	.280
1.200	.339
1.600	.384
2.000	.419
2.400	.445
2.800	.464
3.200	.476
3.600	.480
4.000	.477
4.400	.467
4.800	.447
5.200	.411
5.600	.361
6.000	.301
6.400	.236
6.800	.167
7.200	.099
7.600	.038
8.000	0
L.E. radius: 0.076	

NACA

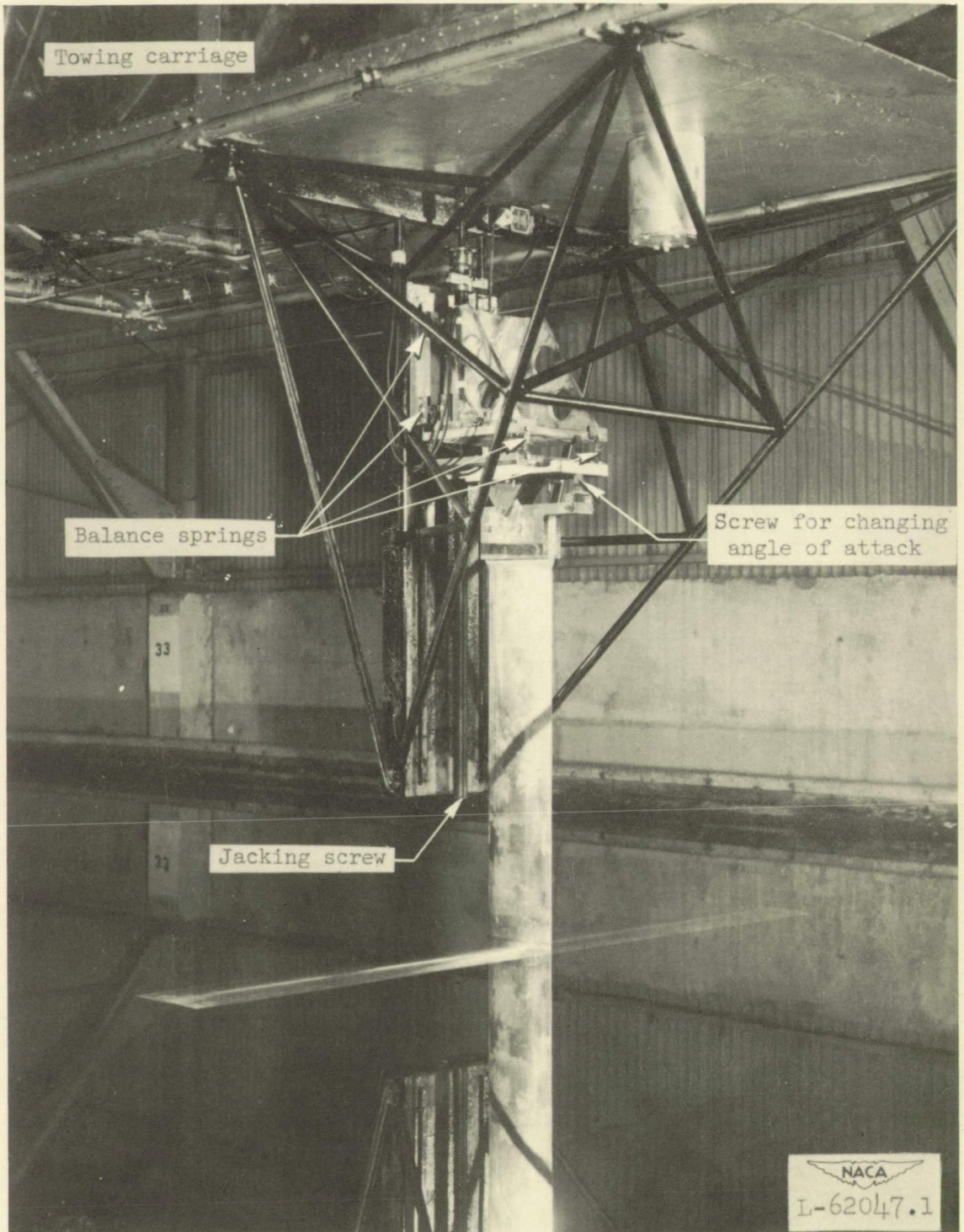
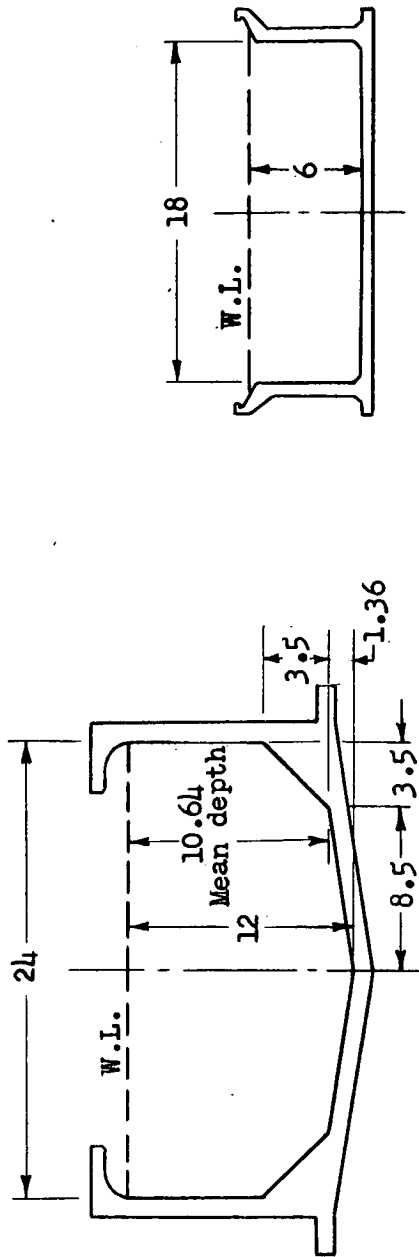


Figure 1.- Test setup showing aspect-ratio-10 hydrofoil and balance attached to towing carriage.



Tank no. 1

Tank no. 2

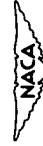
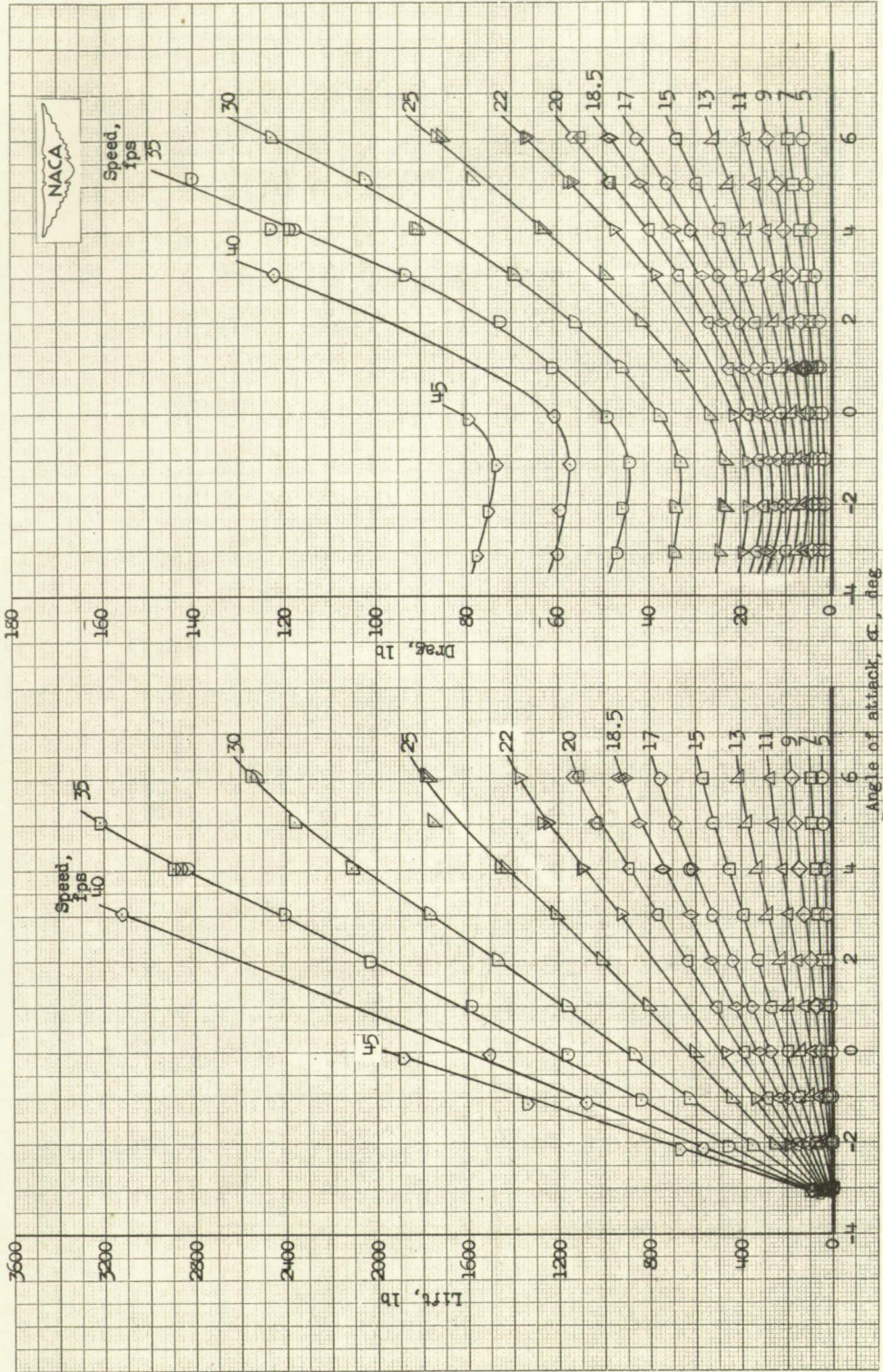
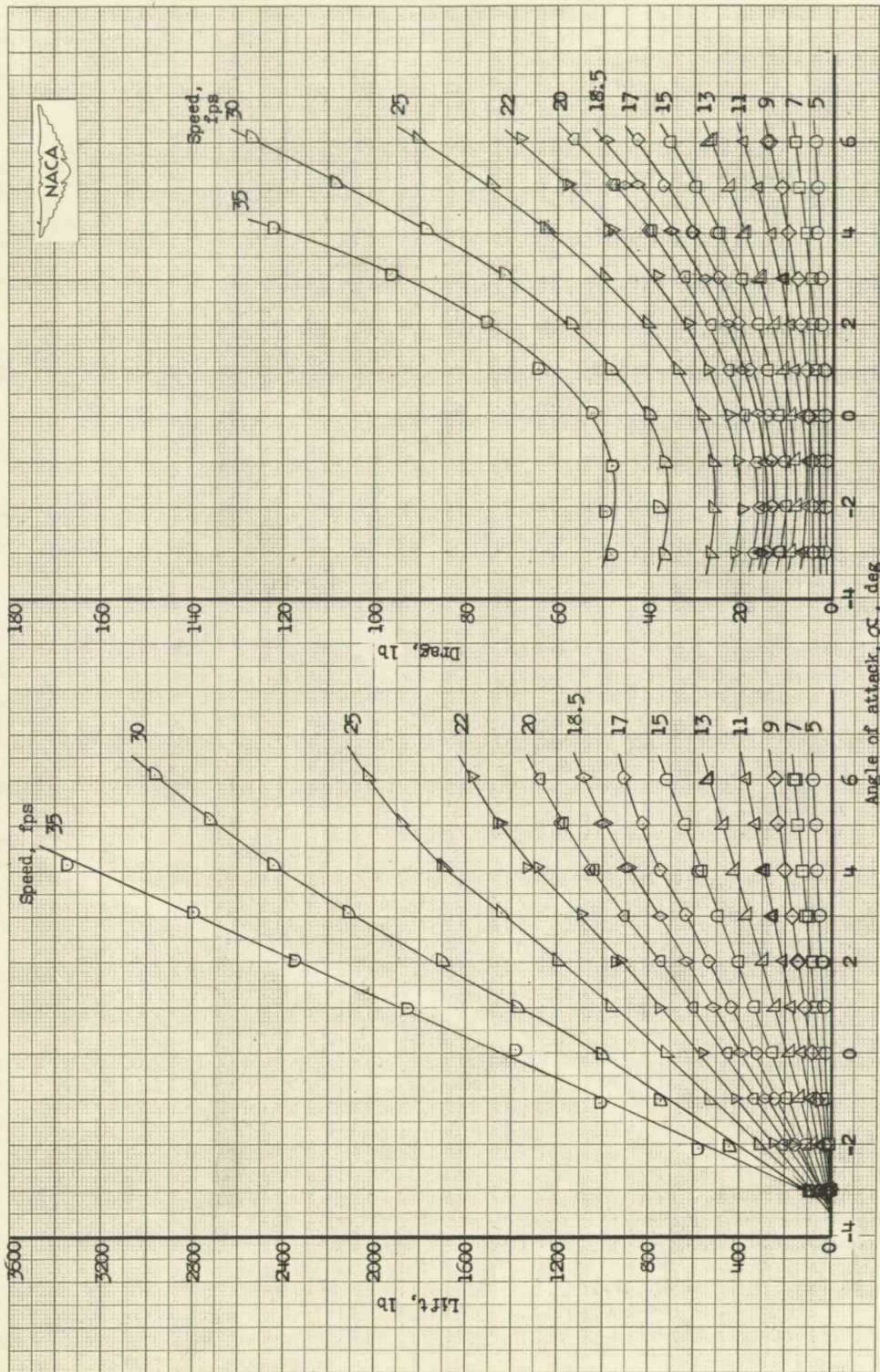


Figure 2.- Sectional details of Langley tanks no. 1 and no. 2.
(Dimensions are in feet.)



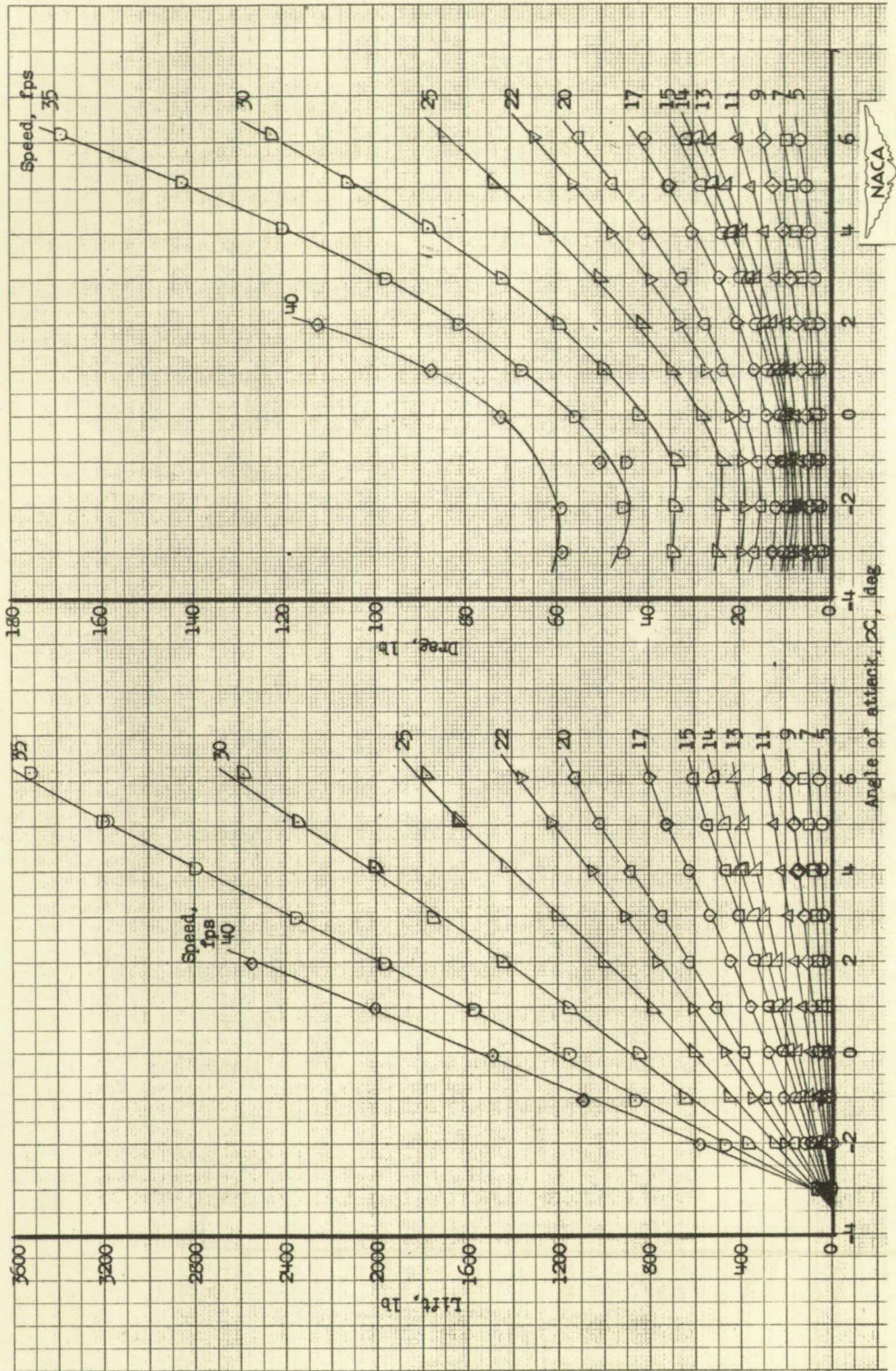
(a) Water depth, 10.64 feet (15.98 chords); depth of submersion, 0.84 chord.

Figure 3.- Lift and drag of the hydrofoil.



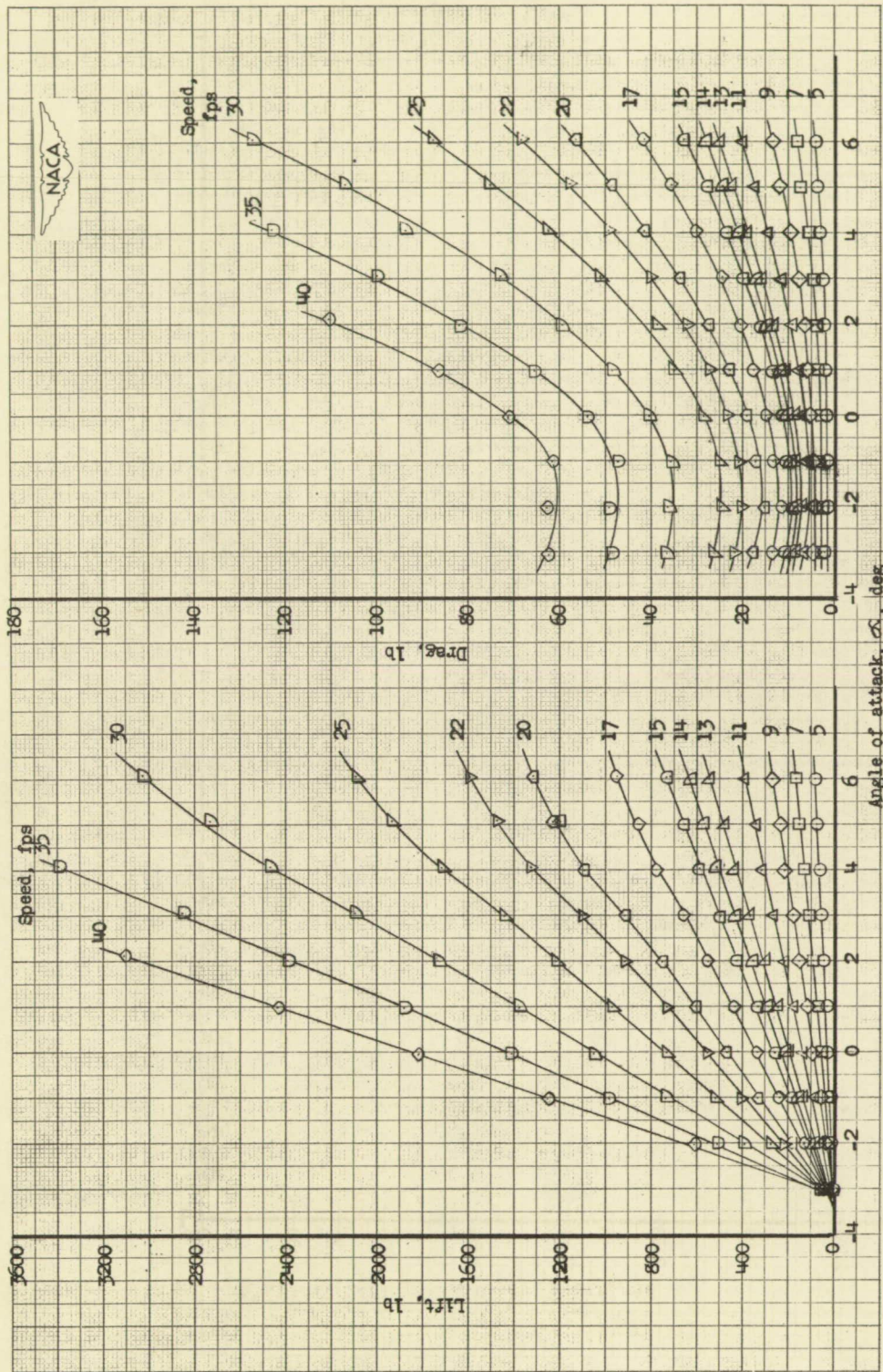
(b) Water depth, 10.64 feet (15.98 chords); depth of submersion, 3.84 chords.

Figure 3.- Continued.



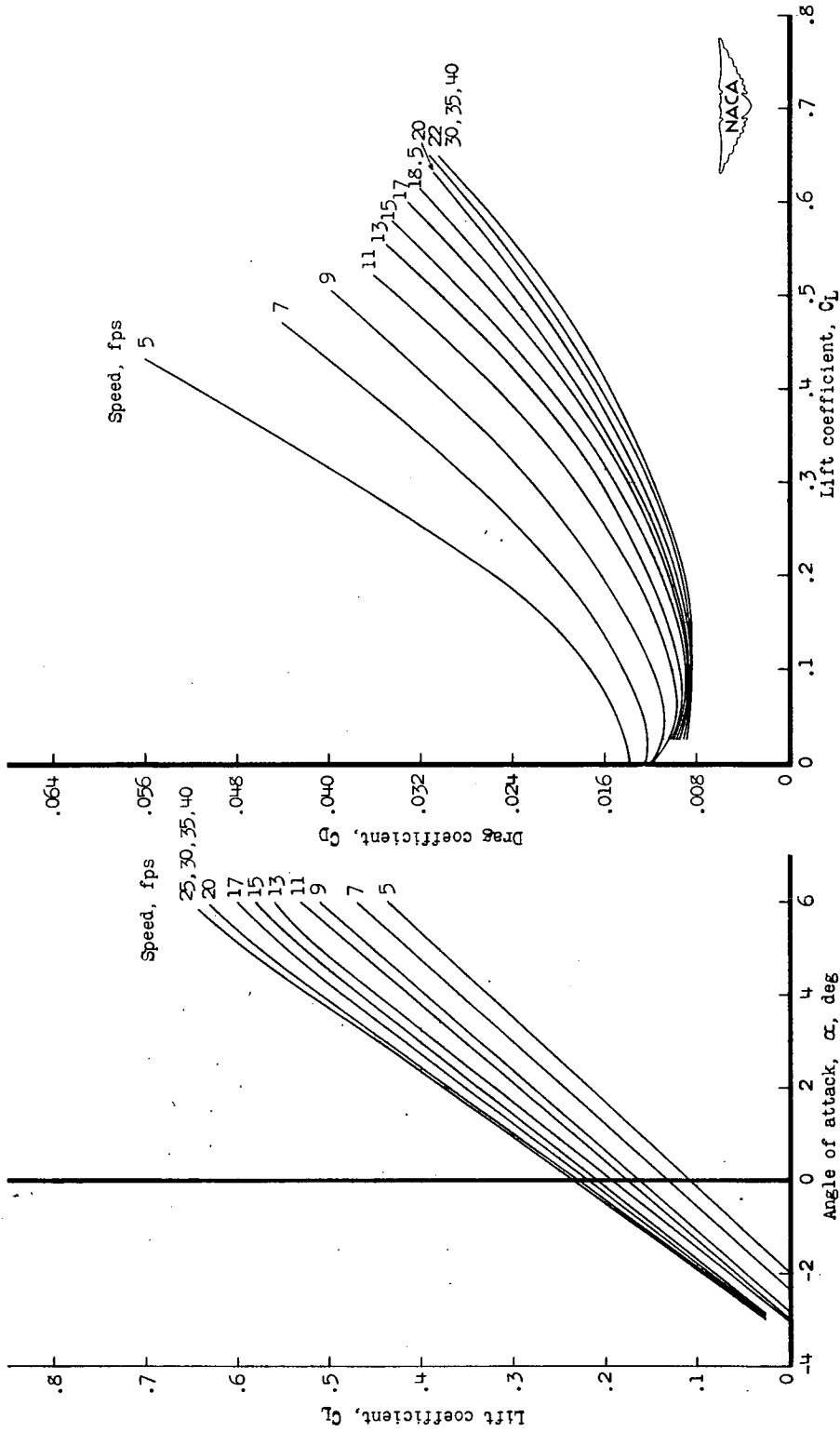
(c) Water depth, 6.0 feet (9.0 chords); depth of submersion, 0.84 chord.

Figure 3.- Continued.



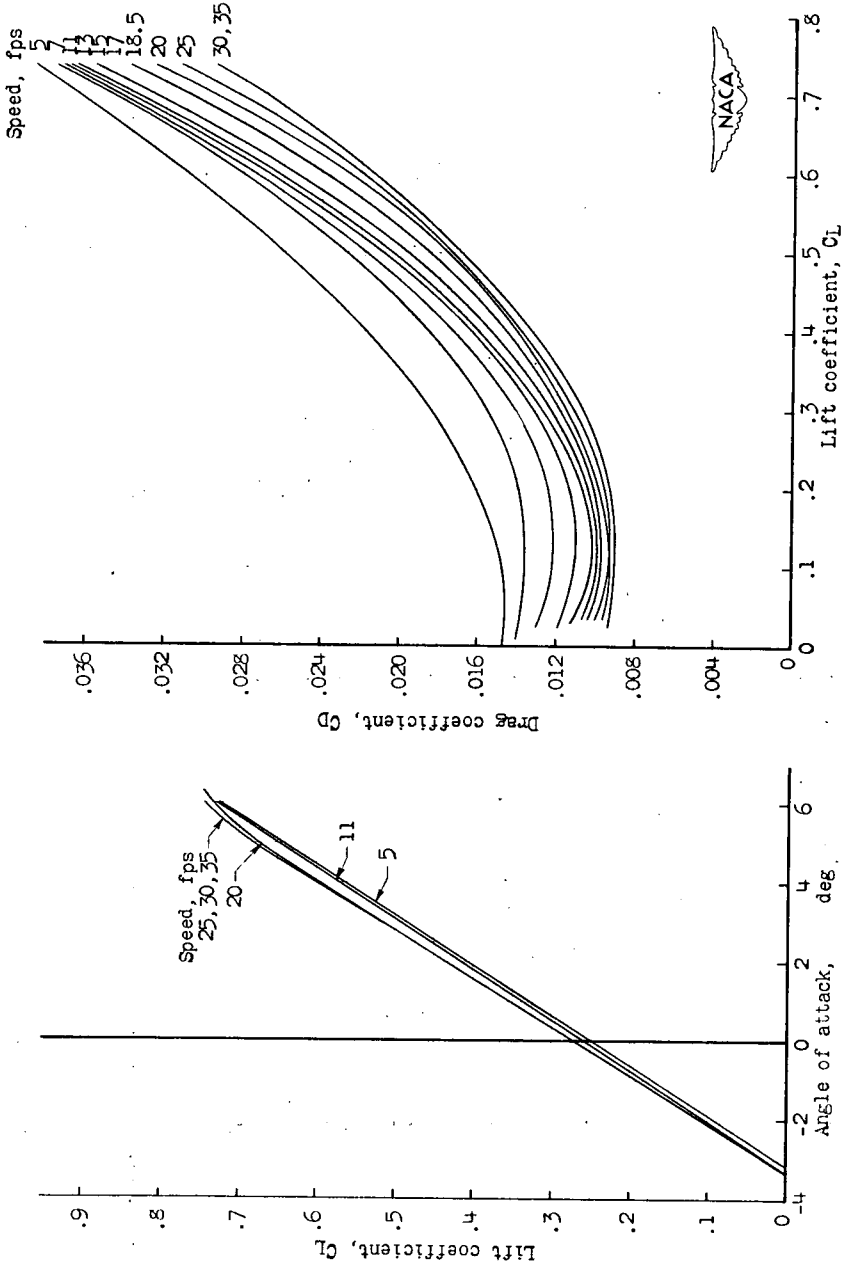
(d) Water depth, 6.0 feet (9.0 chords); depth of submersion, 3.84 chords.

Figure 3.- Concluded.



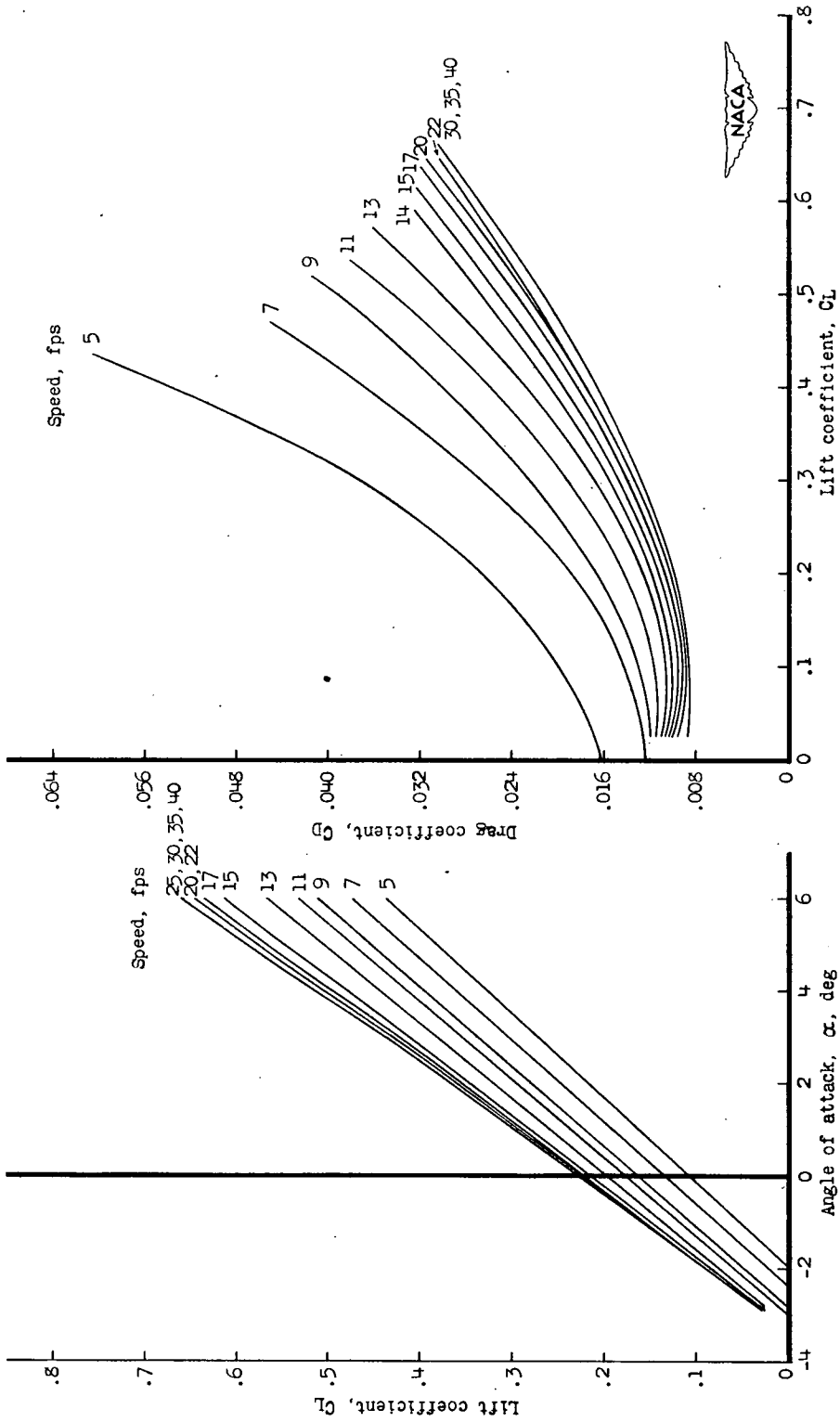
(a) Water depth, 10.64 feet (15.98 chords); depth of submersion, 0.84 chord.

Figure 4.- Lift and drag coefficients of the hydrofoil.



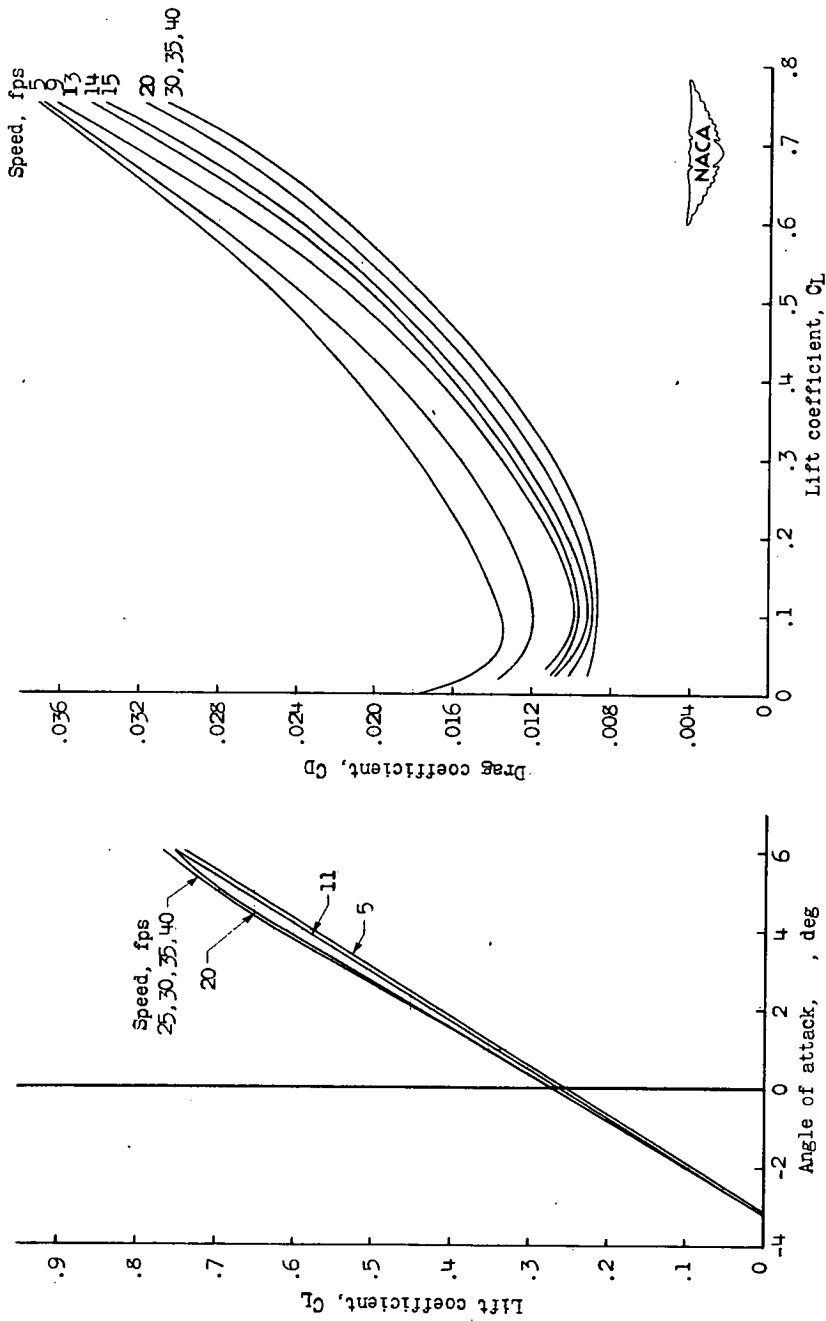
(b) Water depth, 10.64 feet (15.98 chords); depth of submersion, 3.84 chords.

Figure 4.- Continued.



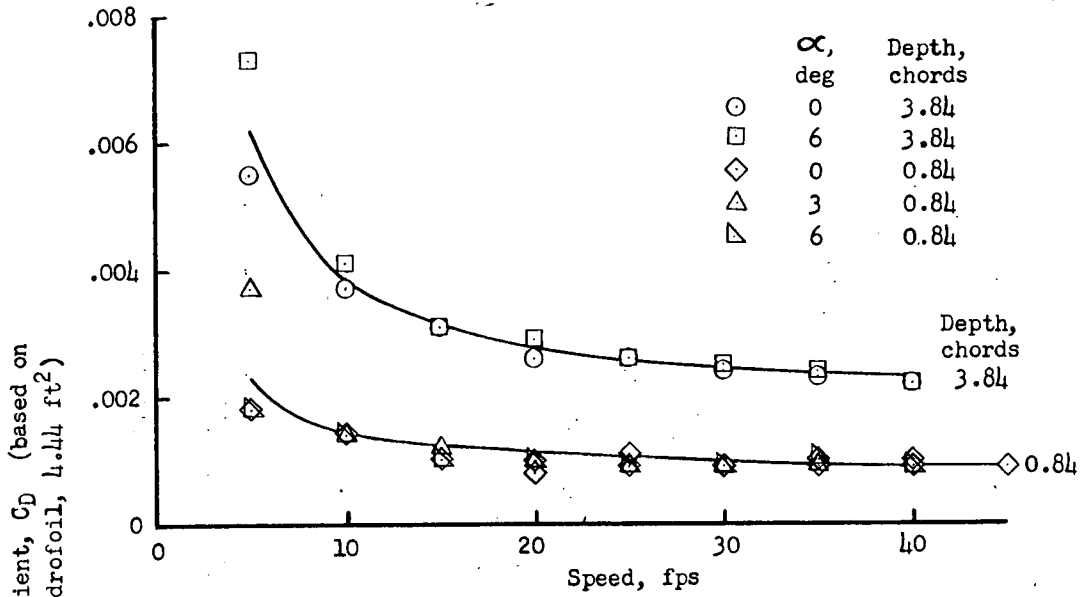
(c) Water depth, 6.0 feet (9.0 chords); depth of submersion, 0.84 chord.

Figure 4.- Continued.

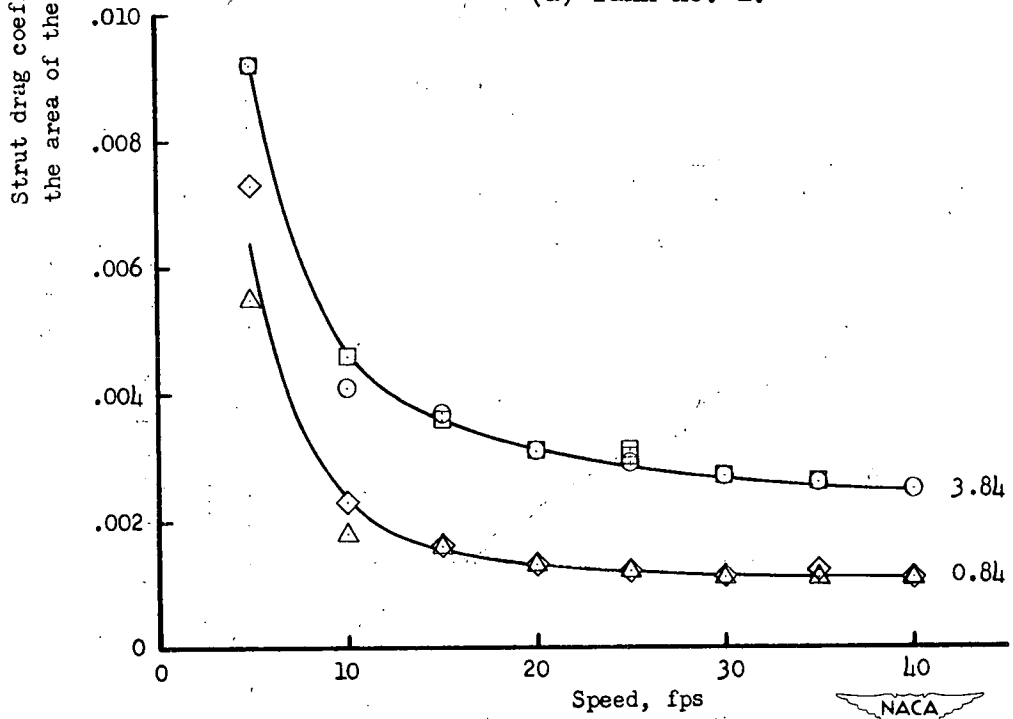


(d) Water depth, 6.0 feet (9.0 chords); depth of submersion, 3.84 chords.

Figure 4.- Concluded.



(a) Tank no. 1.



(b) Tank no. 2.

Figure 5.- Variation of strut drag coefficient with speed and depth of hydrofoil submergence.



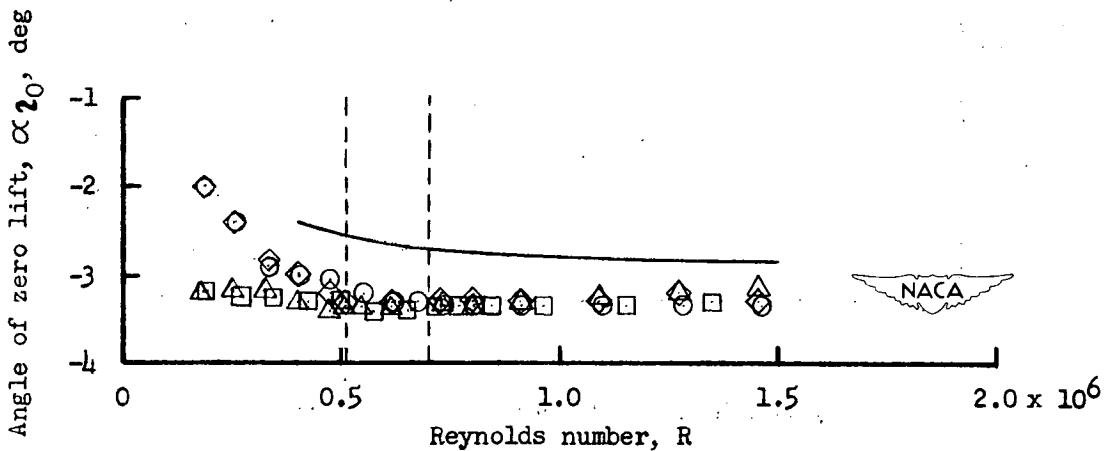
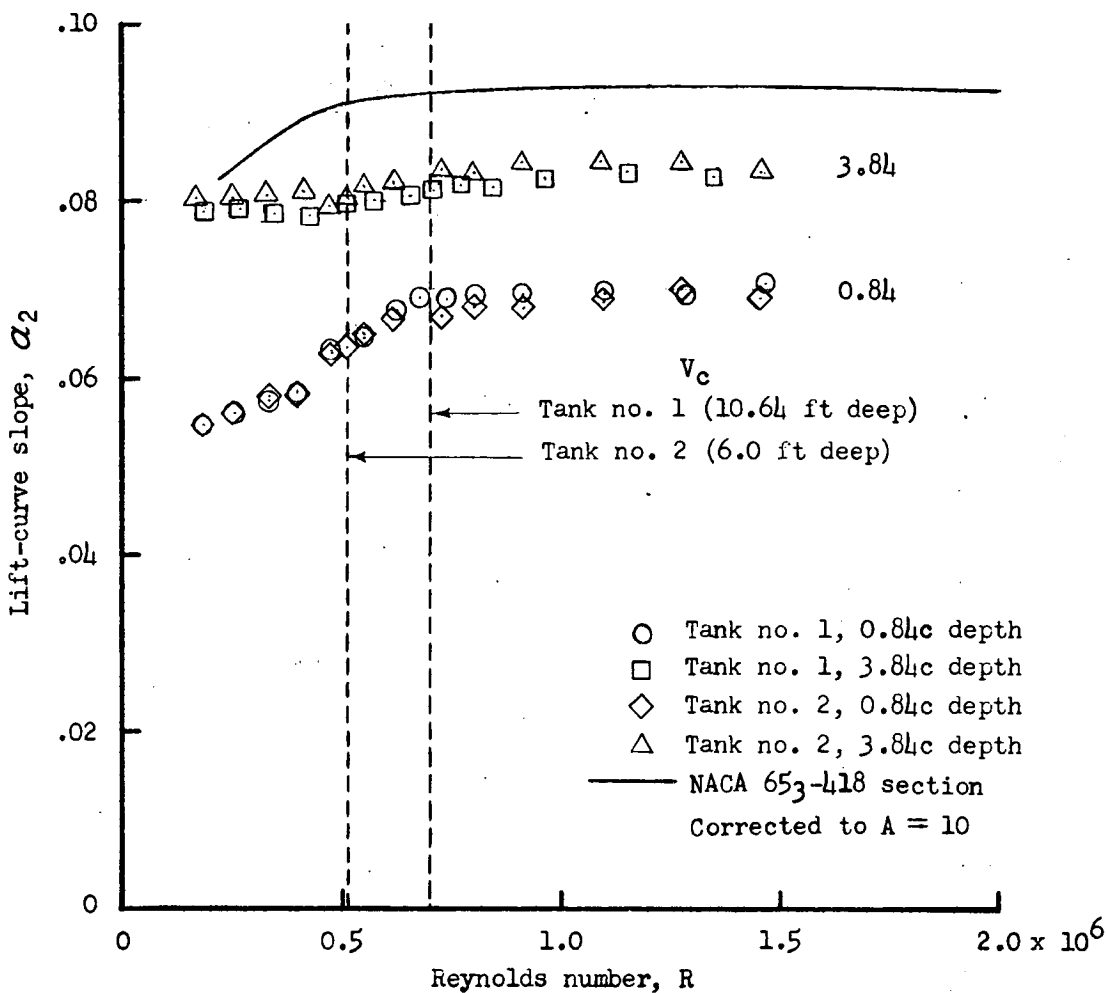
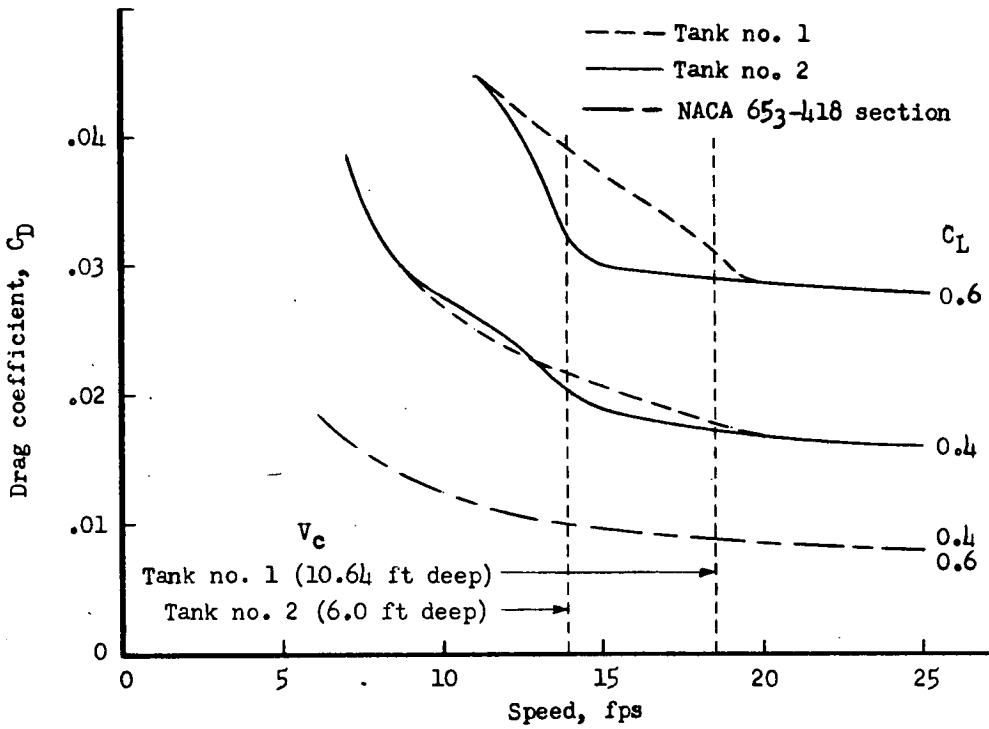
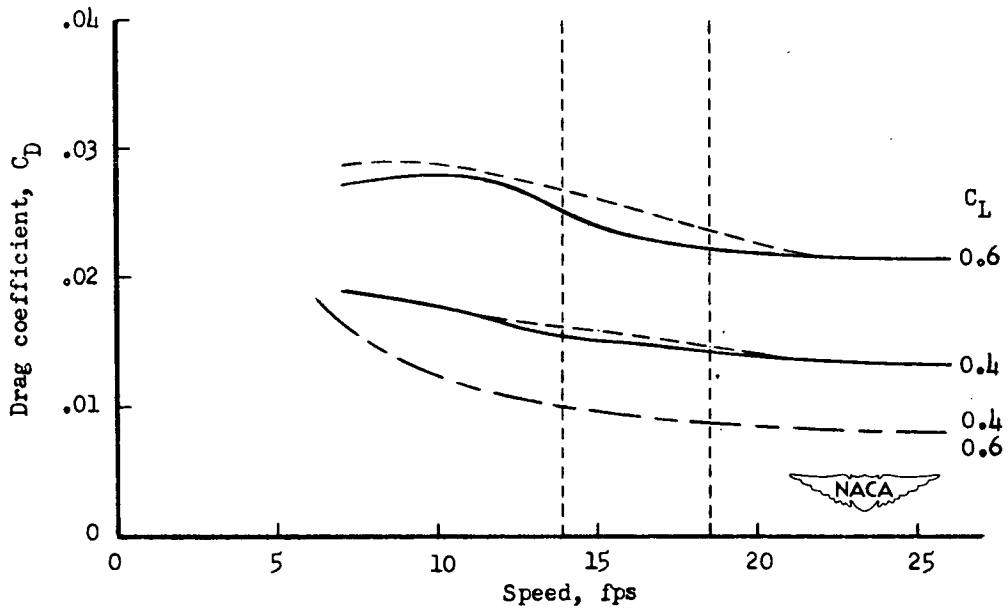


Figure 6.- Variation of lift-curve slope and angle of zero lift with Reynolds number.



(a) Depth of submergence, 0.84 chord.



(b) Depth of submergence, 3.84 chords.

Figure 7.- Variation of drag coefficient with speed for constant lift coefficient.

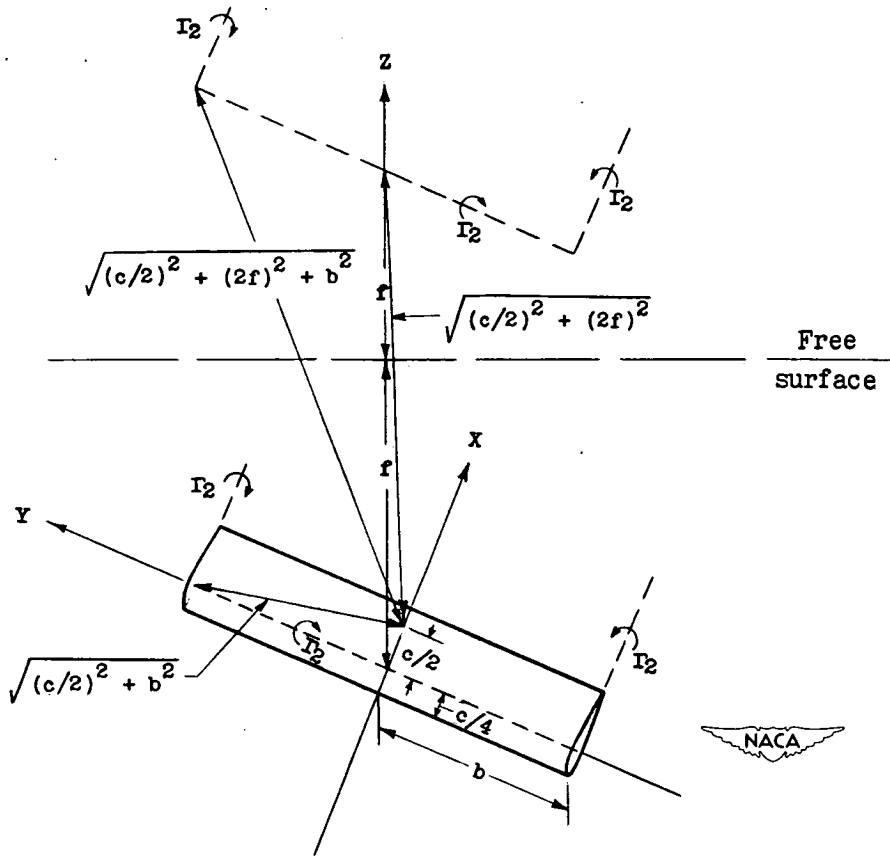


Figure 8.- Horseshoe-vortex arrangement that satisfies the free-surface boundary.

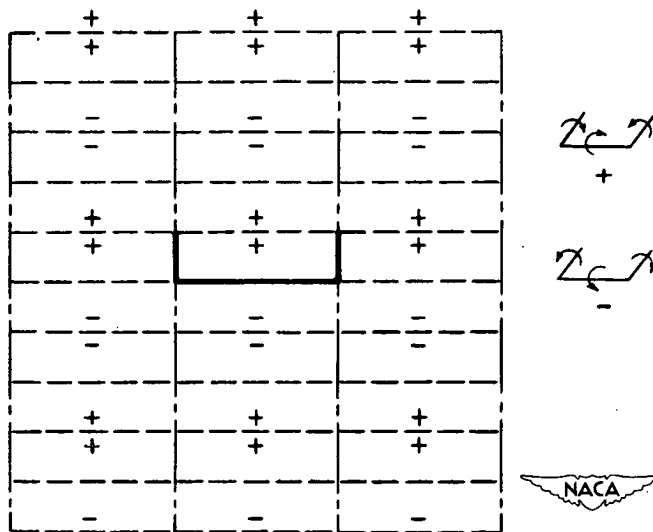
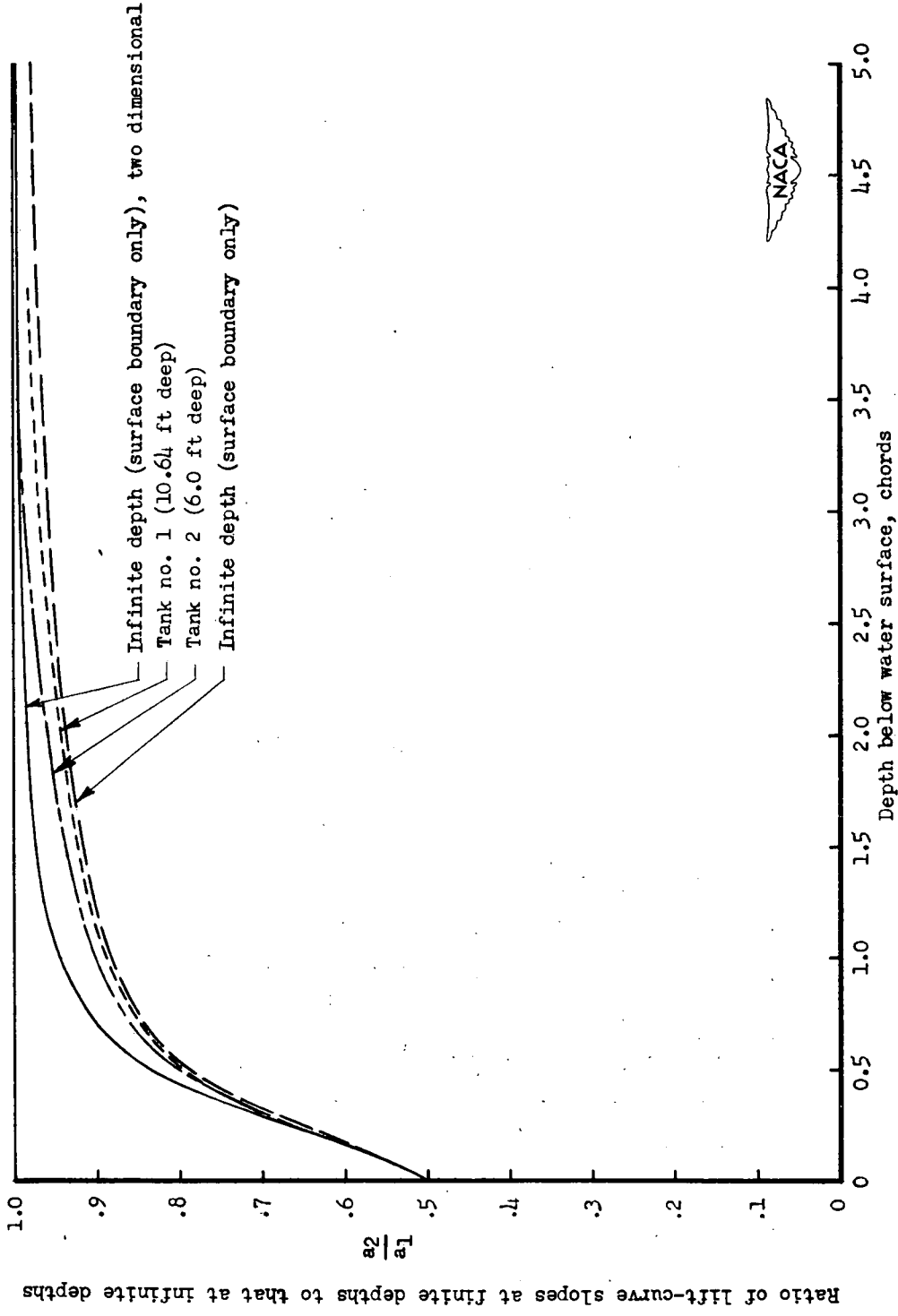


Figure 9.- Horseshoe-vortex arrangement that satisfactorily approximates the tank boundary conditions.

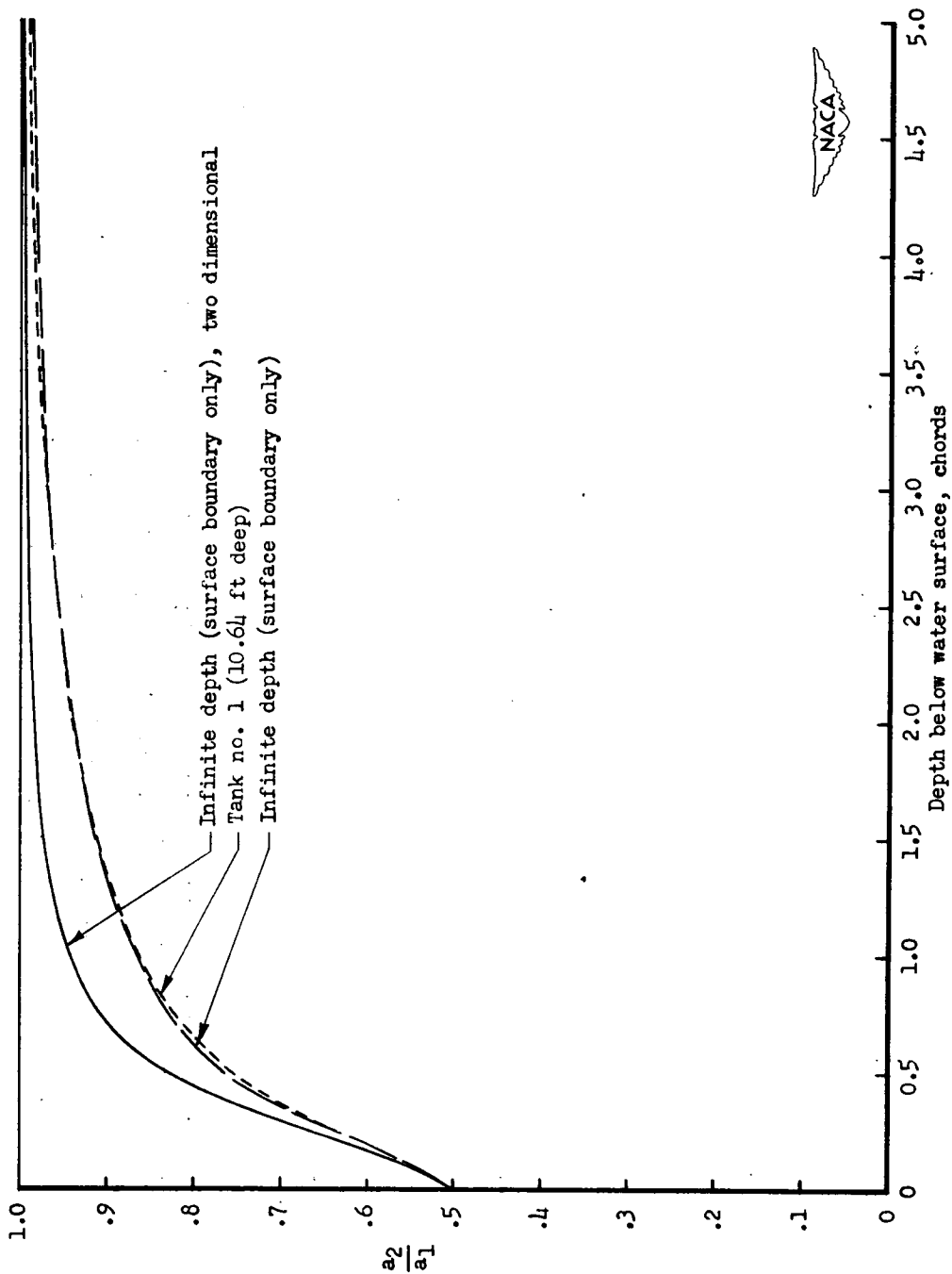


Ratio of lift-curve slopes at finite depths to that at infinite depths



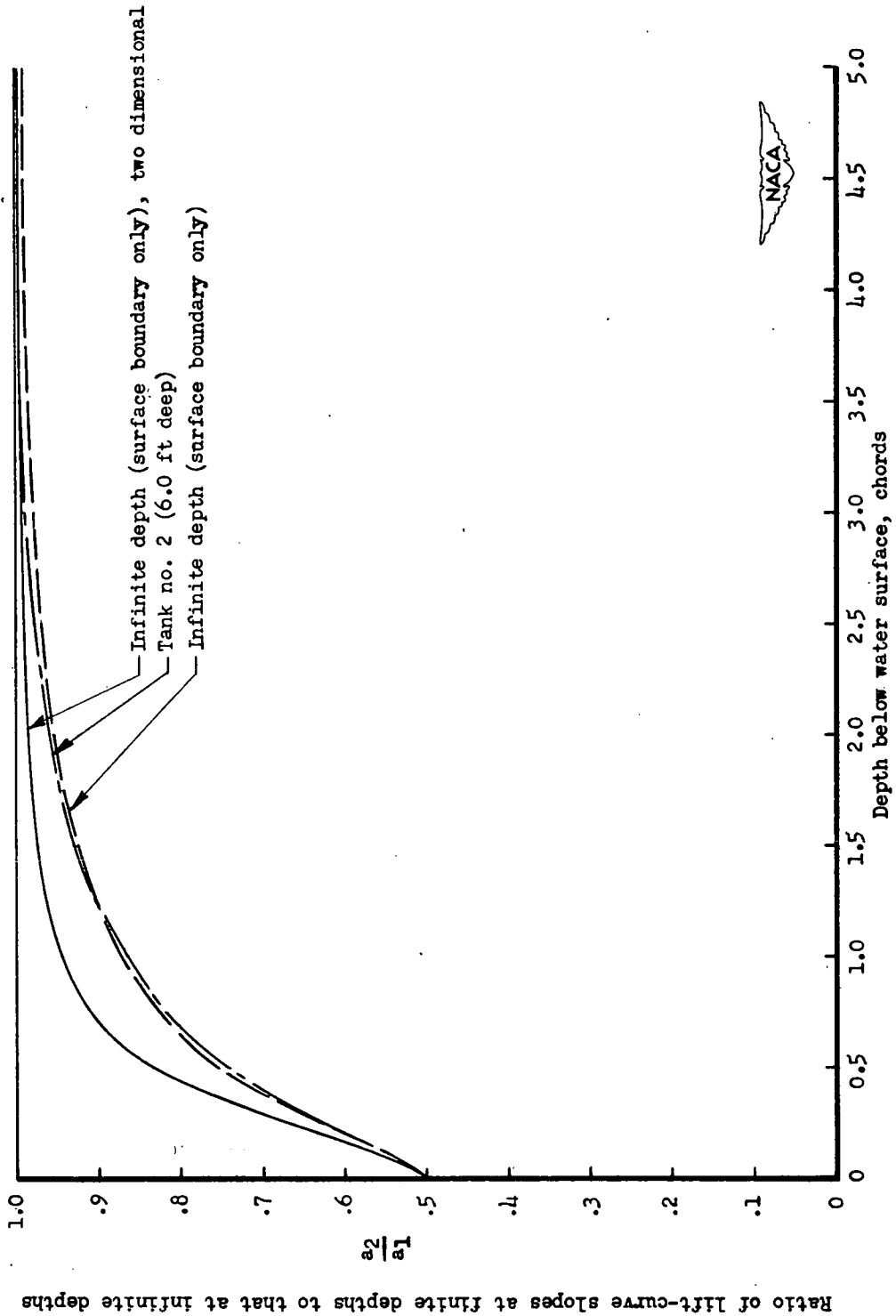
(a) Aspect ratio, 10; chord, 0.667 foot.

Figure 10.- Effect of depth on lift-curve slope.



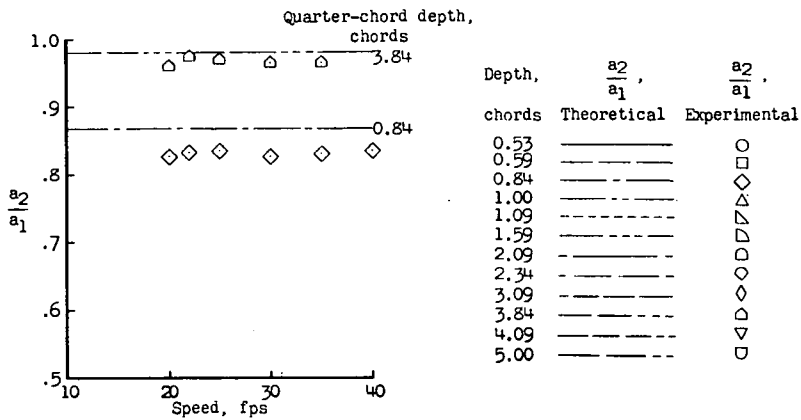
(b) Aspect ratio, 6; chord, 0.417 foot.

Figure 10.- Continued.

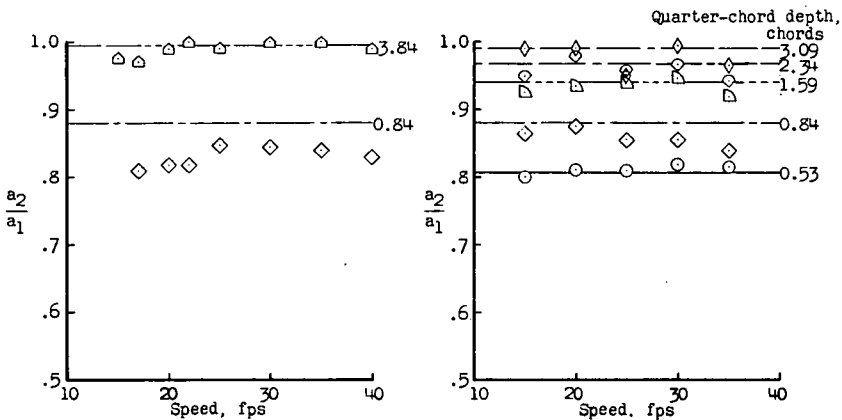


(c) Aspect ratio, 4; chord, 0.667 foot.

Figure 10.- Concluded.

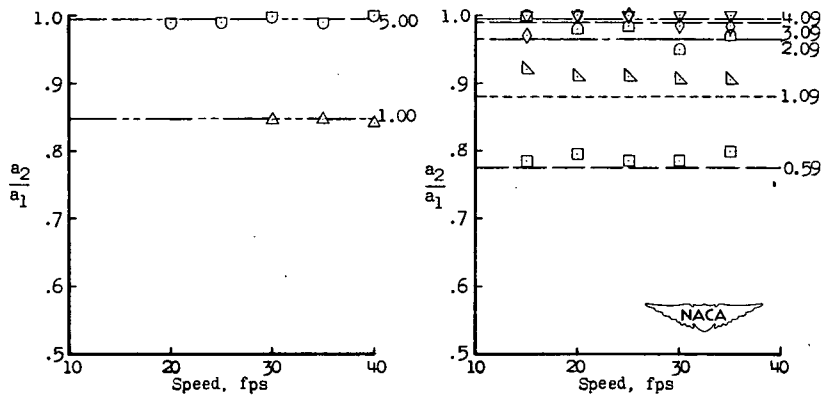


(a) Aspect ratio, 10; tank no. 1.



(b) Aspect ratio, 10; tank no. 2.

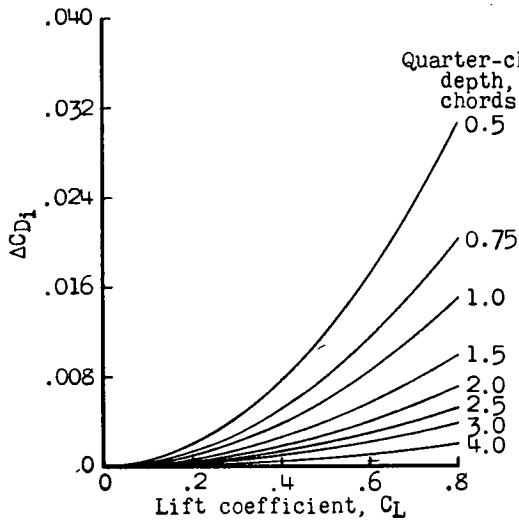
(c) Aspect ratio, 10; tank no. 2 (ref. 2).



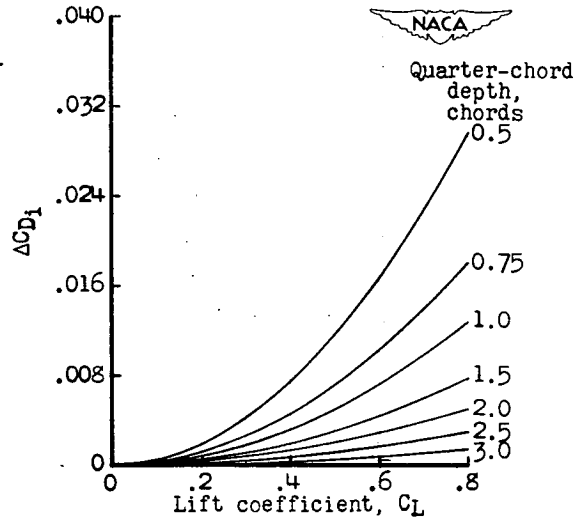
(d) Aspect ratio, 6; tank no. 1 (ref. 10).

(e) Aspect ratio, 4; tank no. 2 (ref. 1).

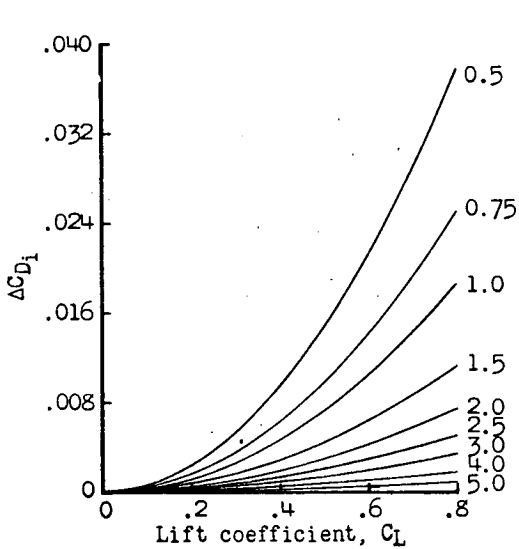
Figure 11.- Comparison of experimental and theoretical ratio of lift-curve slopes for aspect ratios 10, 6, and 4.



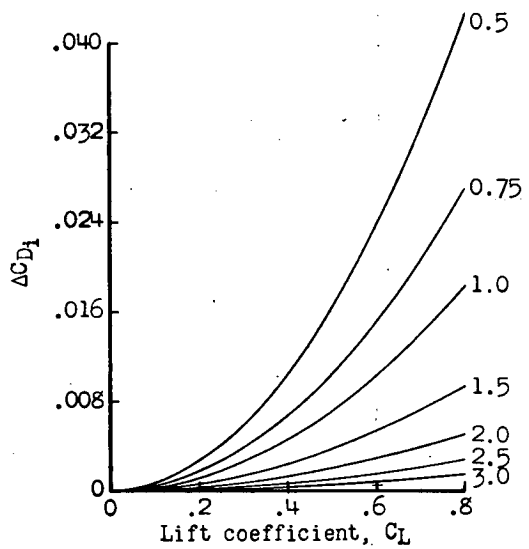
(a) Aspect ratio, 10; tank no. 1.



(b) Aspect ratio, 10; tank no. 2.

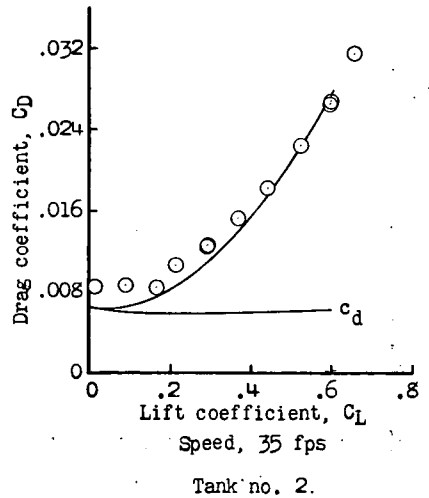
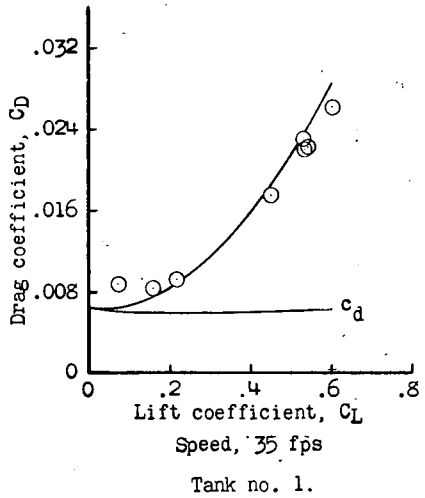
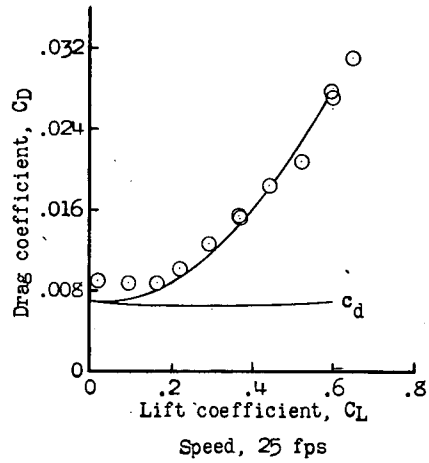
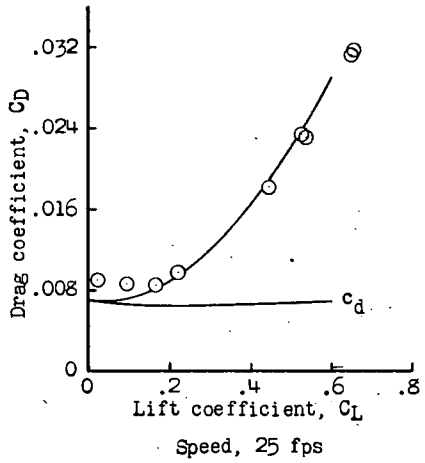
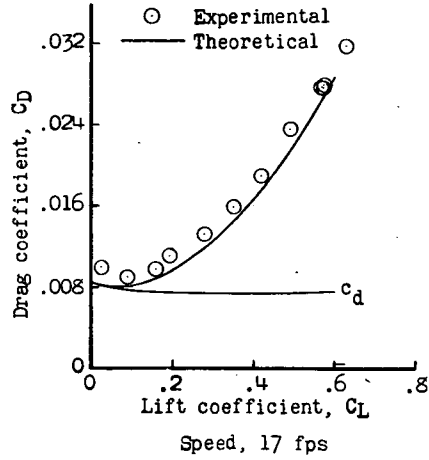
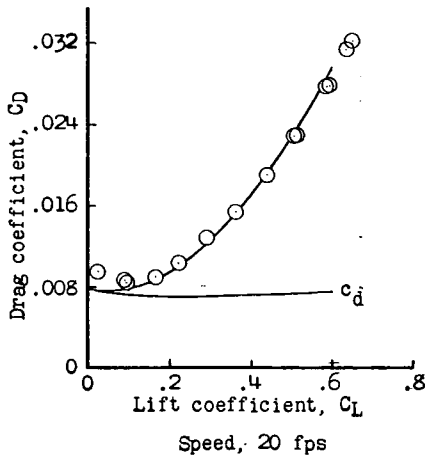


(c) Aspect ratio, 6; tank no. 1.



(d) Aspect ratio, 4; tank no. 2.

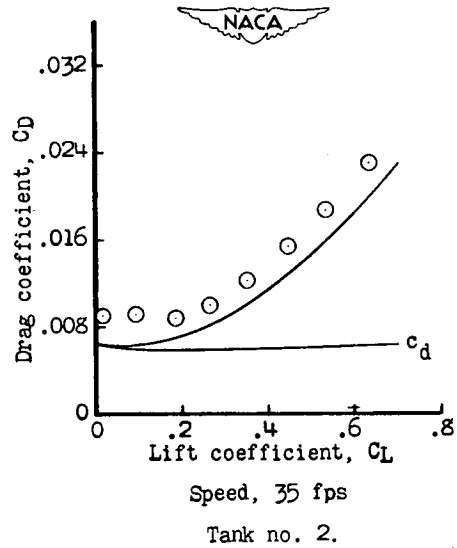
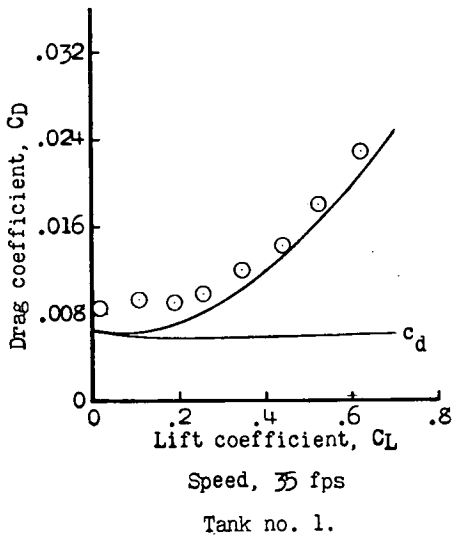
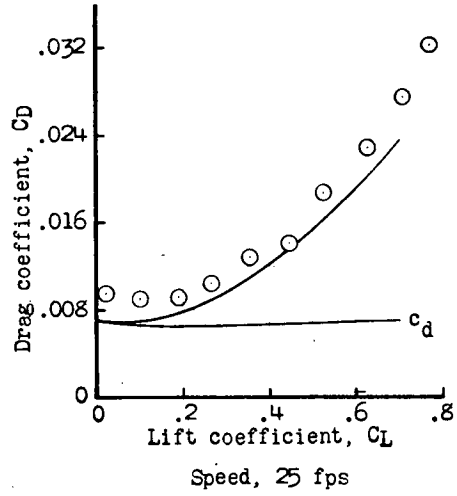
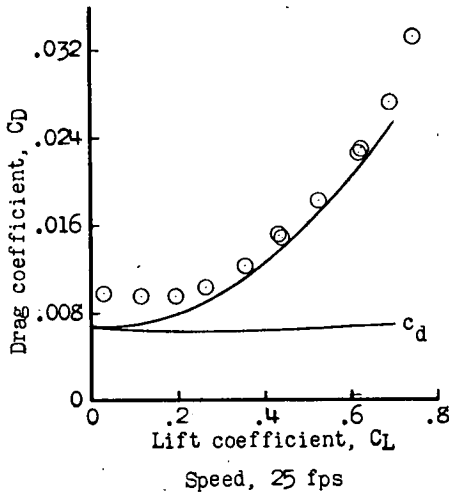
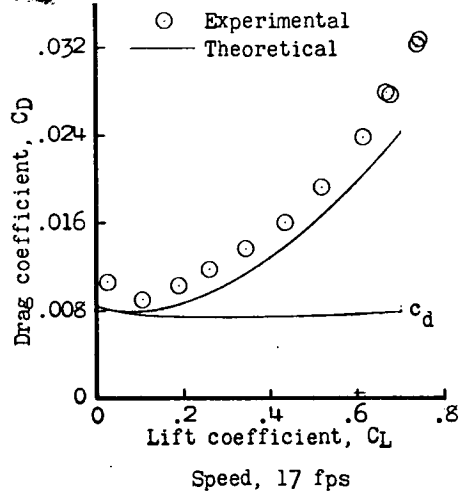
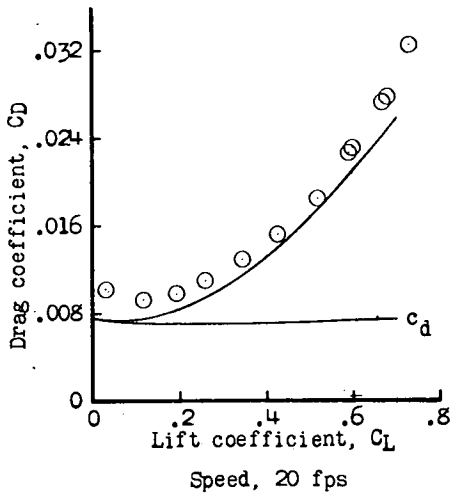
Figure 12.- Variation of induced drag coefficient due to the hydrofoil vortex images with lift coefficient for hydrofoils of aspect-ratios 10, 6, and 4.



(a) Depth, 0.84 chord.

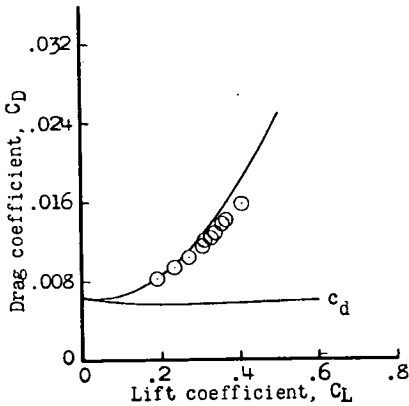


Figure 13.- Comparison of experimental and theoretical drag coefficients for aspect-ratio-10 hydrofoil.

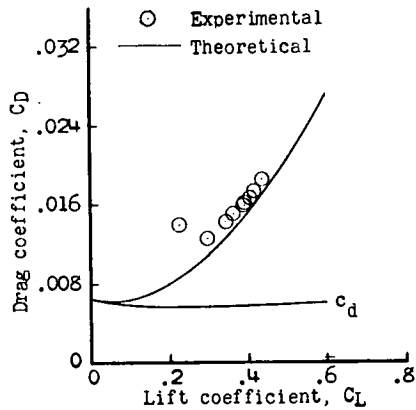


(b) Depth, 3.84 chords.

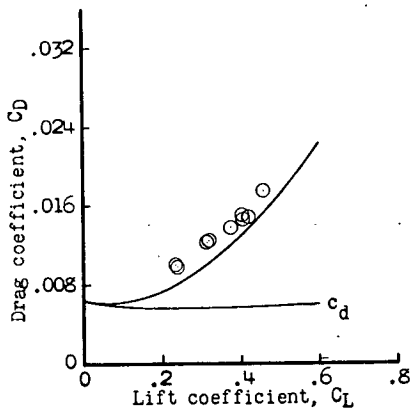
Figure 13.- Concluded.



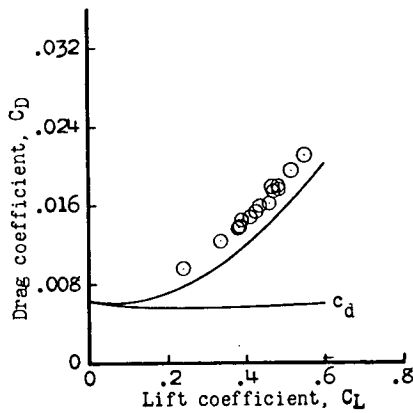
(a) Depth, 0.53 chord.



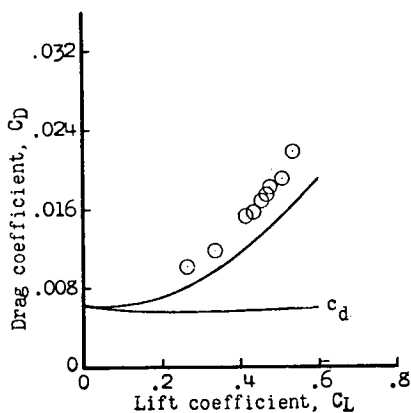
(b) Depth, 0.84 chord.



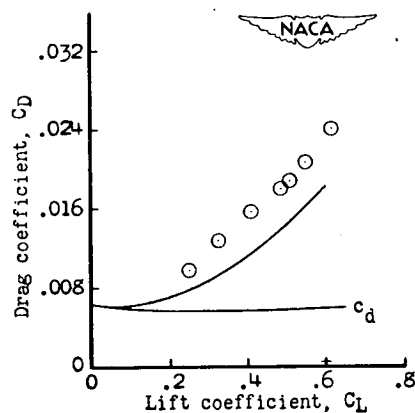
(c) Depth, 1.59 chords.



(d) Depth, 2.34 chords.

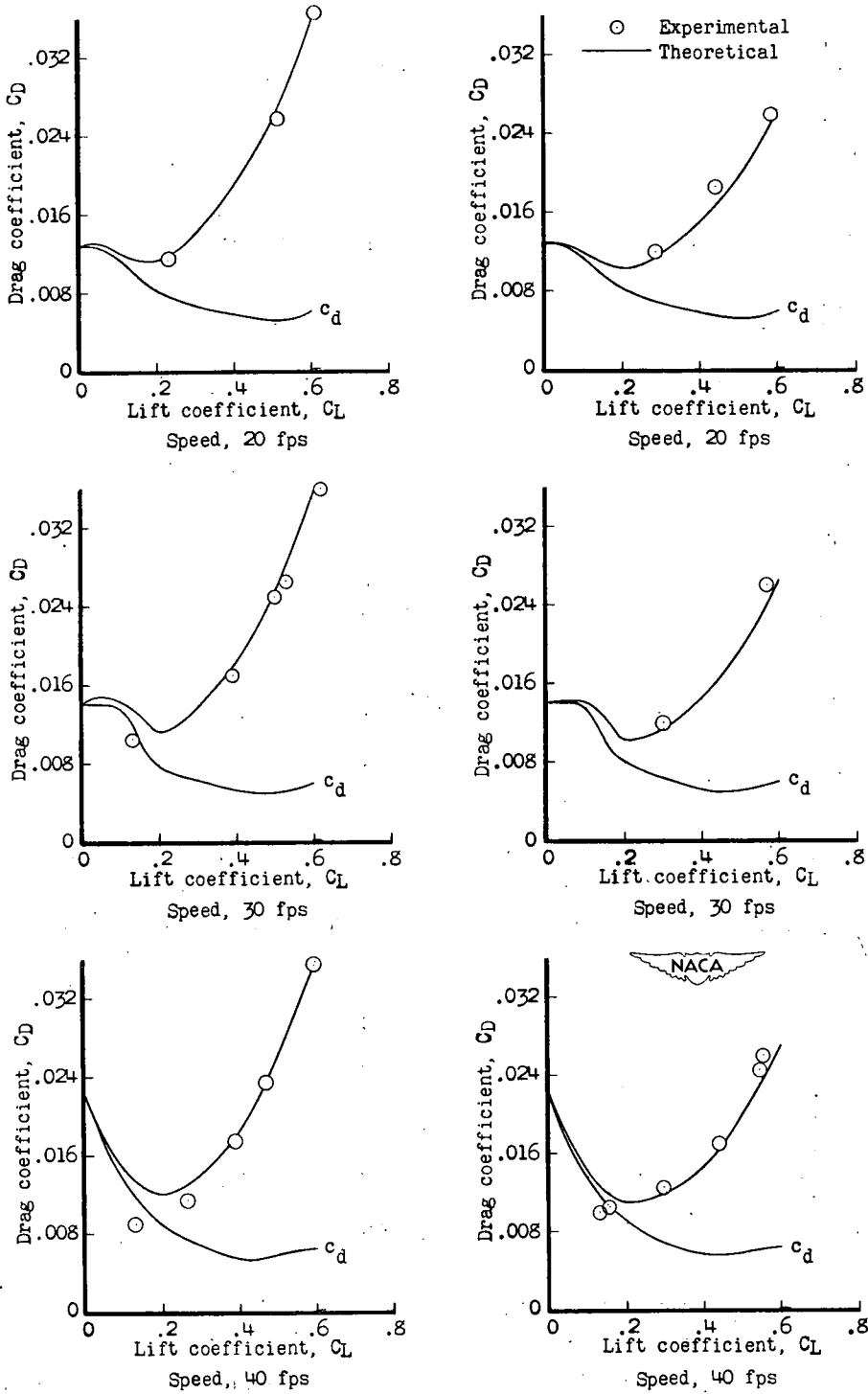


(e) Depth, 3.09 chords.



(f) Depth, 3.84 chords.

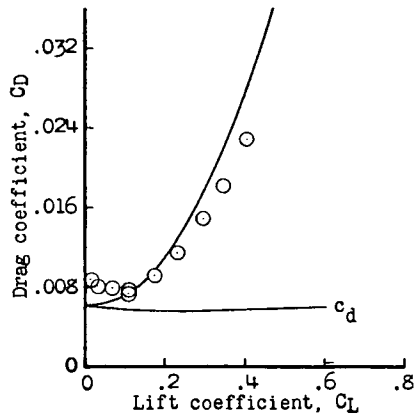
Figure 14.- Comparison of experimental and theoretical drag coefficients for aspect-ratio-10 hydrofoil (see ref. 1). Speed, 25 fps.



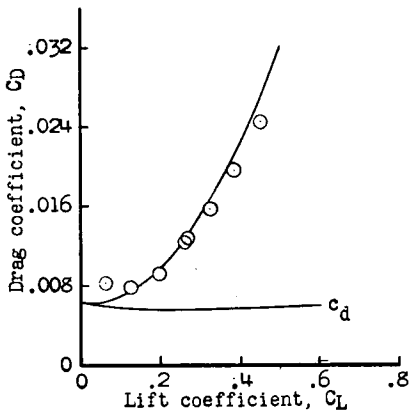
(a) Depth, 1.0 chords.

(b) Depth, 5.0 chords.

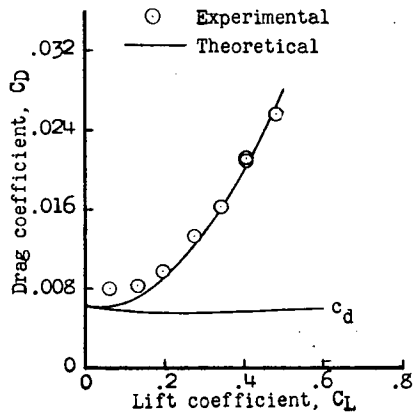
Figure 15.- Comparison of experimental and theoretical drag coefficients for aspect-ratio-6 hydrofoil (see ref. 10).



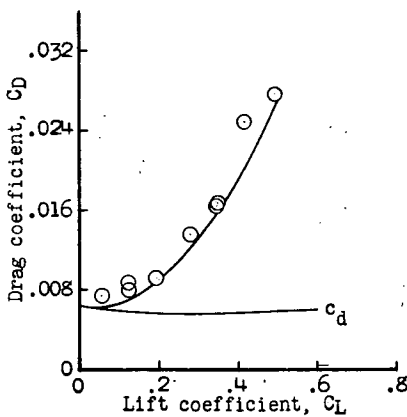
(a) Depth, 0.59 chord.



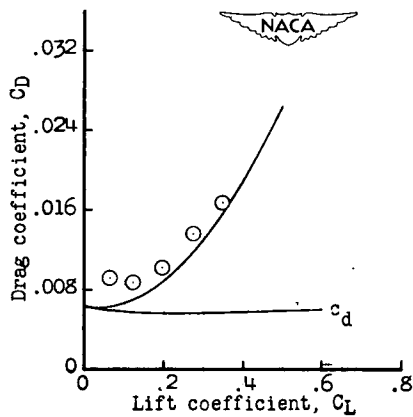
(b) Depth, 1.09 chords.



(c) Depth, 2.09 chords.

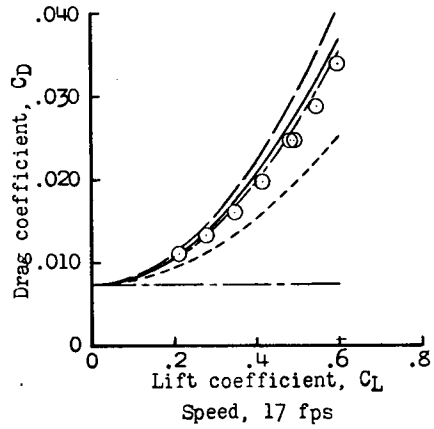
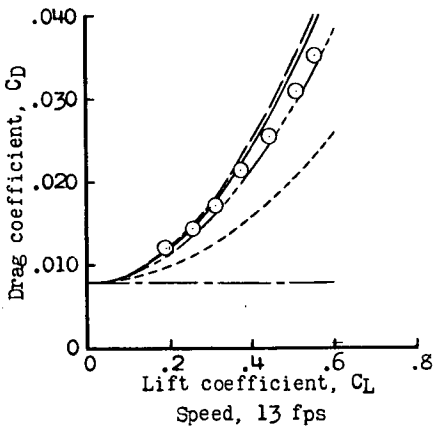
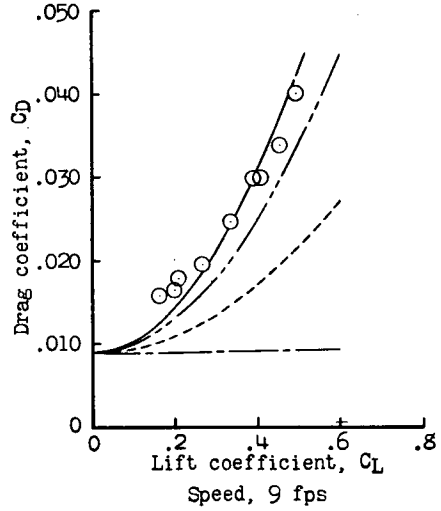
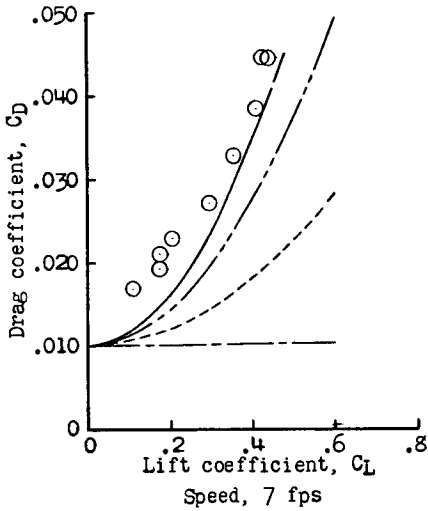
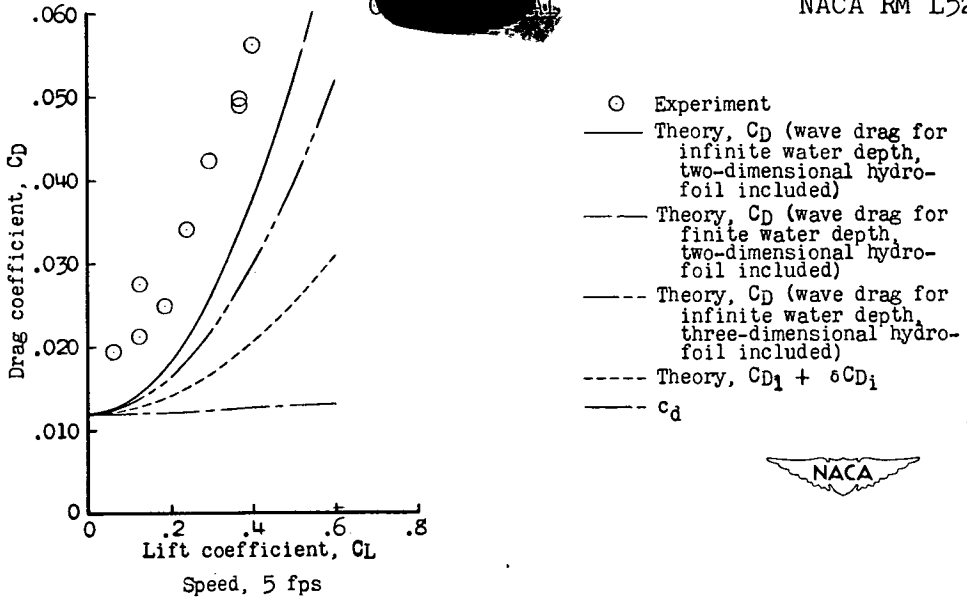


(d) Depth, 3.09 chords.



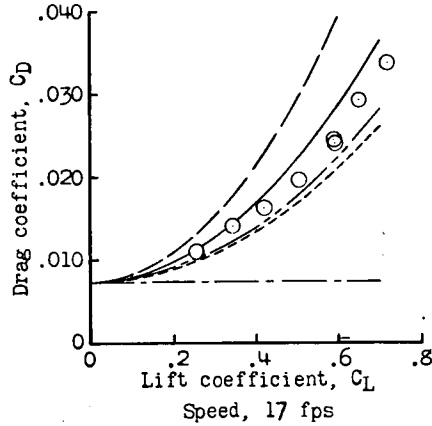
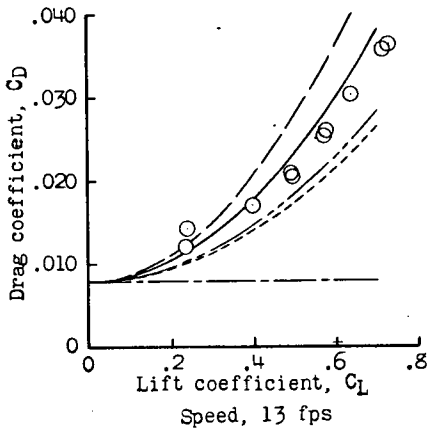
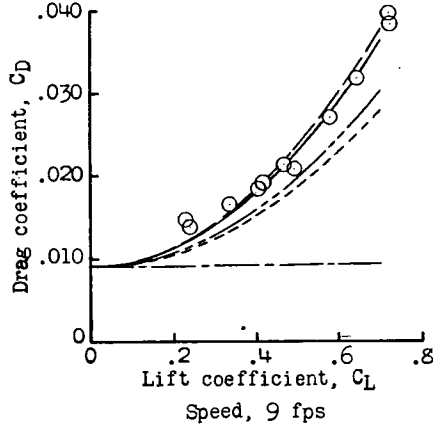
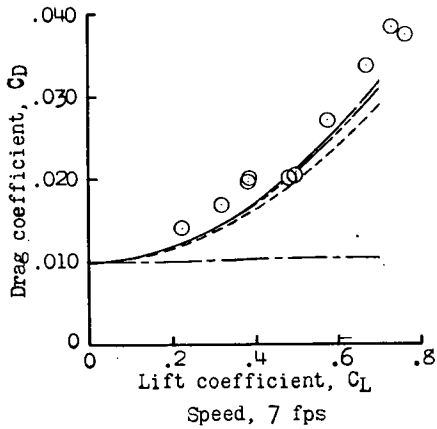
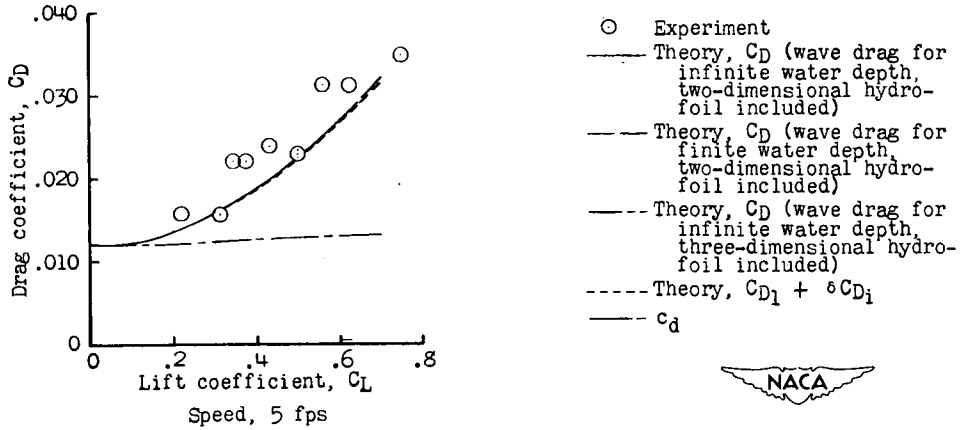
(e) Depth, 4.09 chords.

Figure 16.- Comparison of experimental and theoretical drag coefficients for aspect-ratio-4 hydrofoil (see ref. 2). Speed, 25 fps.



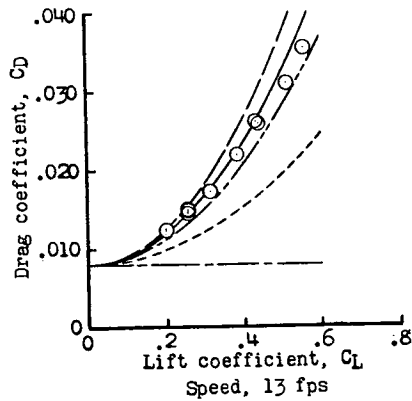
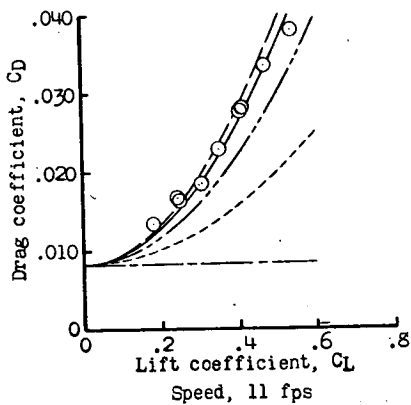
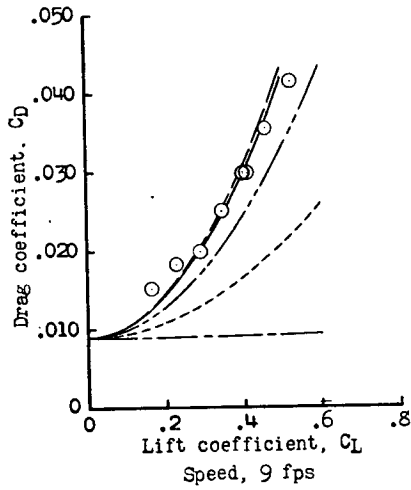
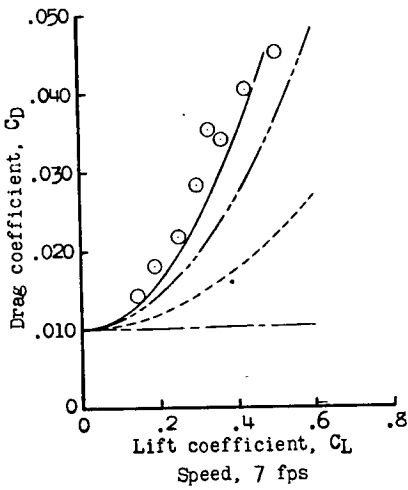
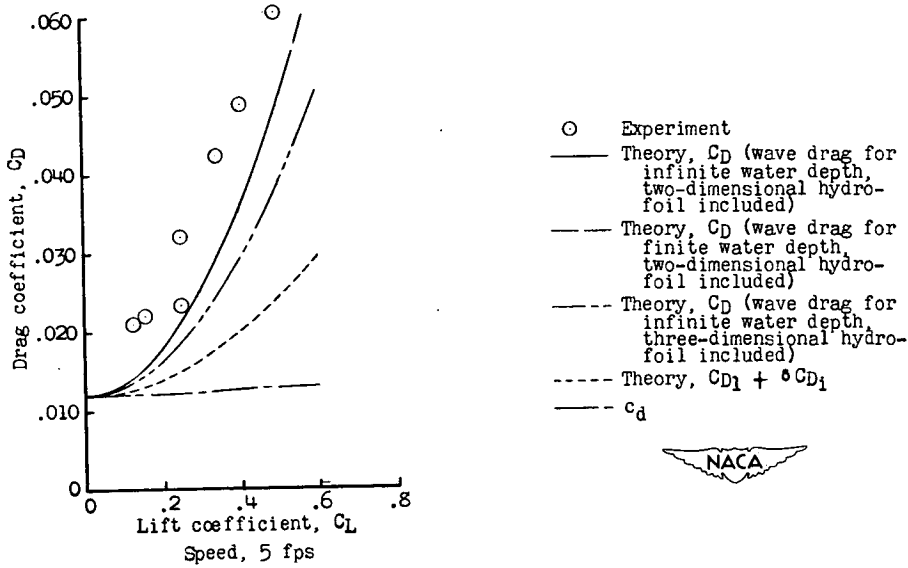
(a) Depth, 0.84 chord.

Figure 17.- Comparison of experimental and theoretical drag coefficients for aspect-ratio-10 hydrofoil. Water depth, 10.64 feet (tank no. 1).



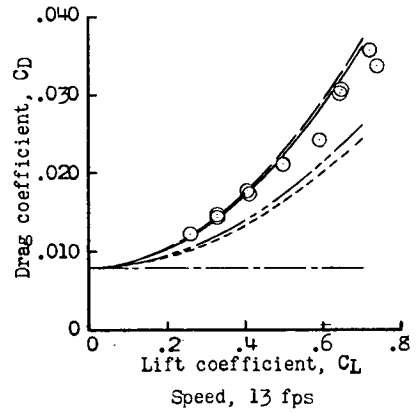
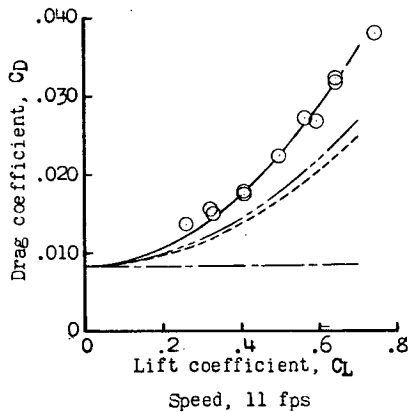
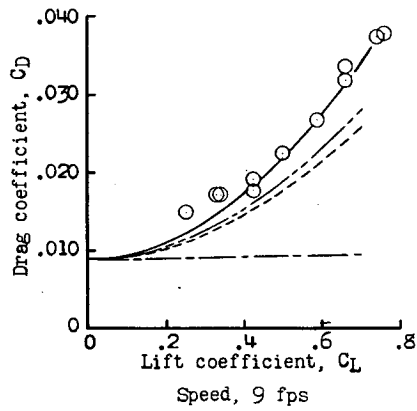
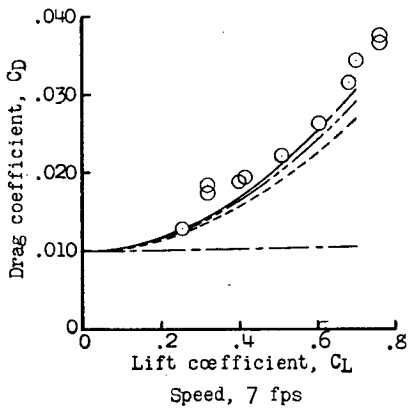
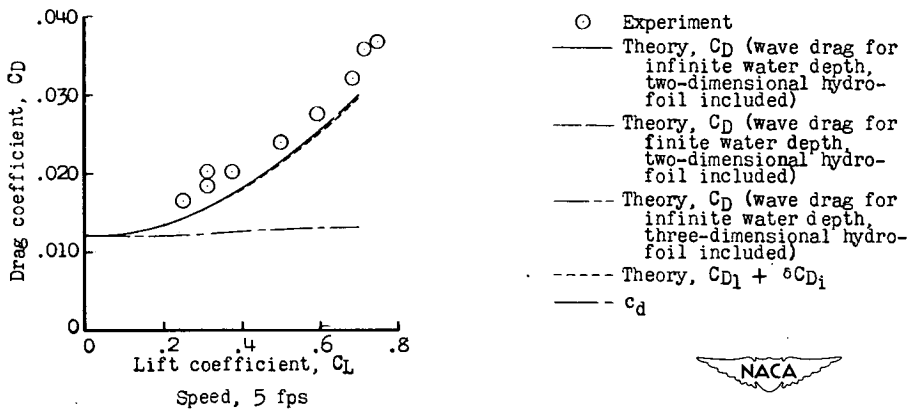
(b) Depth, 3.84 chords.

Figure 17.- Concluded.



(a) Depth, 0.84 chord.

Figure 18.- Comparison of experimental and theoretical drag coefficients for aspect-ratio-10 hydrofoil. Water depth, 6.0 feet (tank no. 2).



(b) Depth, 3.84 chords.

Figure 18.- Concluded.

CONFIDENTIAL

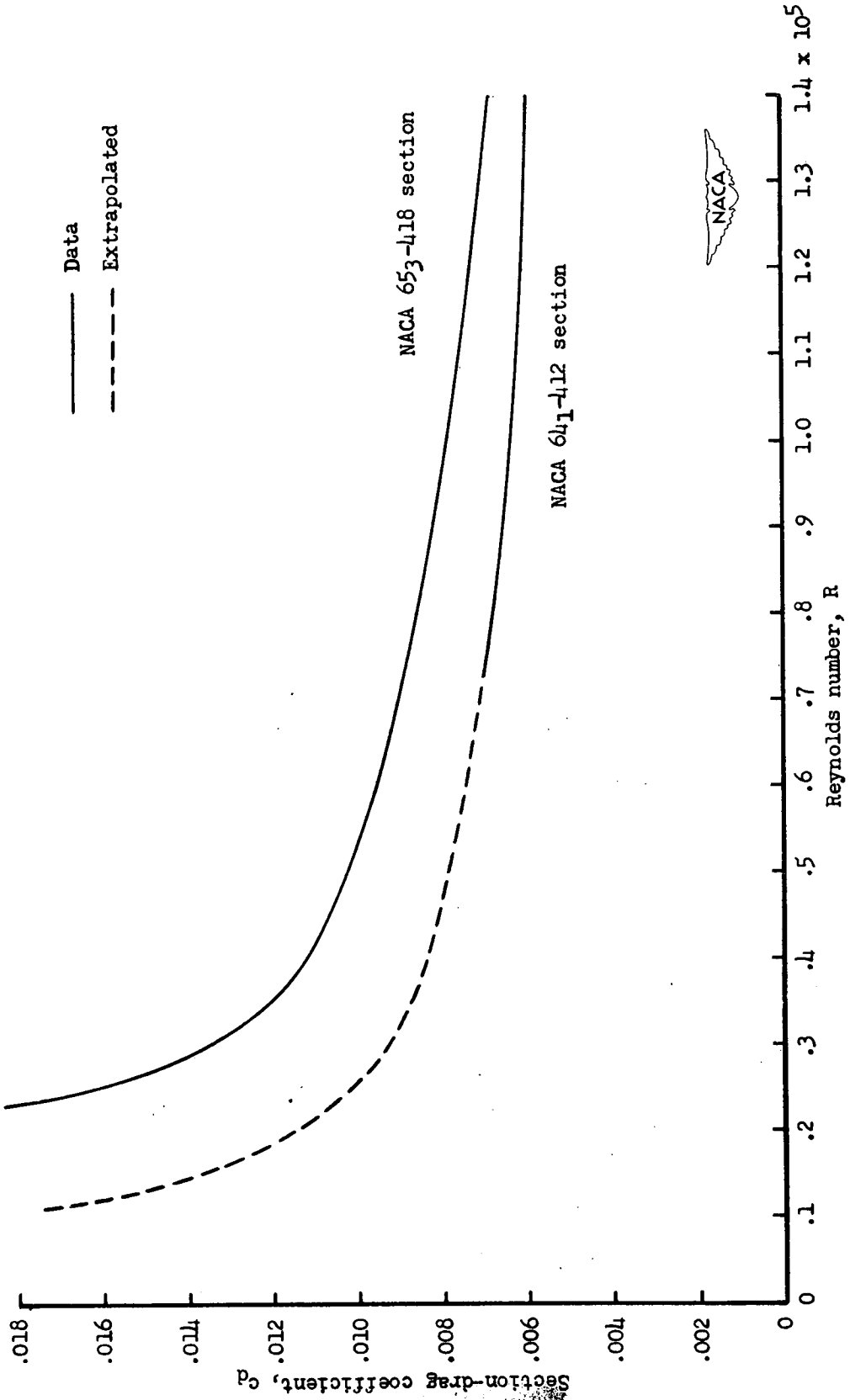


Figure 19.- Variation of section drag coefficient with Reynolds number ($C_L = 0.2$).

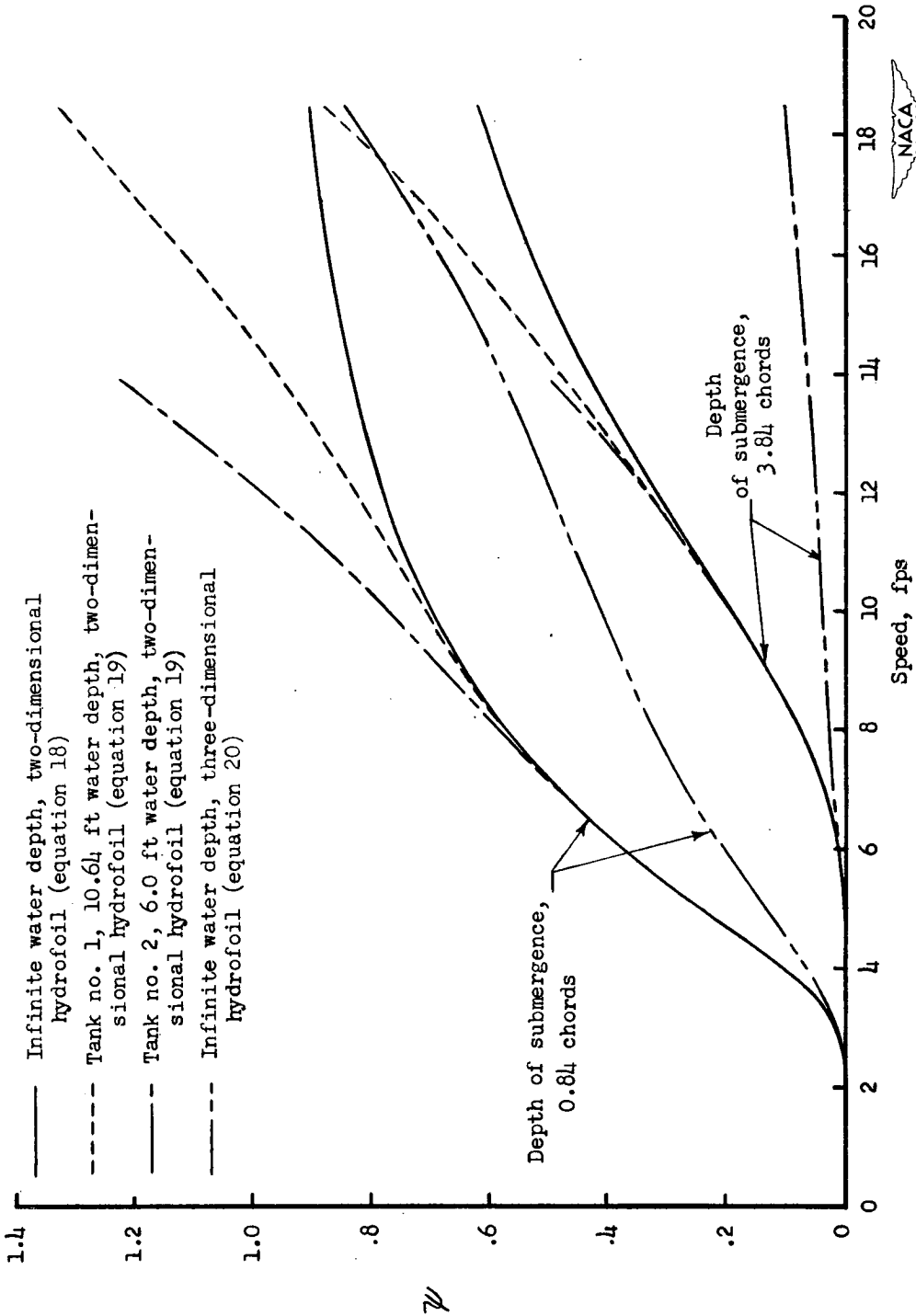


Figure 20.- Variation of ψ (see eq. 17) with speed for infinite water depth and for finite water depth at 0.84- and 3.84-chords hydrofoil submergence.

~~CONFIDENTIAL INFORMATION~~

~~CONFIDENTIAL~~

~~CONFIDENTIAL~~